

metaDMG – A Fast and Accurate

Ancient DNA Damage Toolkit for Metagenomic Data

✉ For correspondence:

christianmichelsen@gmail.com

(CM); mwpedersen@sund.ku.dk

(MW);

tskorneliussen@sund.ku.dk

(TSK).

[†]Authors contributed equally.

Data availability: The source code for metaDMG is available on [Zenodo](#) or at the [Github](#) repository. All code used in the statistical analysis can be found at the following DOI: [10.5281/zenodo.7368194](https://doi.org/10.5281/zenodo.7368194).

Sequencing data and supporting material used in simulations can be found at [ERDA](#).

Funding: CM and TP is funded by the Lundbeck Foundation. MWP is funded by the ERC project LASTJOURNEY (ERC_Adv_834514). TSK is funded by Carlsberg grant CF19-0712.LZ. was funded by Lundbeck Foundation Centre for Disease Evolution: R302-2018-2155

Competing interests: The author declare no competing interests.

- ⁴ Christian Michelsen ^{1,2}  *, Mikkel Winther Pedersen ²  *, Antonio Fernandez-Guerra ² *, Lei Zhao², Troels C. Petersen ¹ *, Thorfinn Sand ⁶ Korneliussen ²  

¹ Niels Bohr Institute, University of Copenhagen, Blegdamsvej 17, 2100 Copenhagen,
⁸ Denmark; ²GLOBE, Section for Geogenetics, Øster Voldgade 5-7, 1350, Copenhagen,
Denmark

Abstract

- ¹² **1. Motivation** Under favourable conditions DNA molecules can persist for hundreds of thousands of years. Such genetic remains make up invaluable resources to study past assemblages, populations, and even the evolution of species. However, DNA is subject to degradation, and hence over time decrease to ultra low concentrations which makes it highly prone to contamination by modern sources. Strict precautions are therefore necessary to ensure that DNA from modern sources does not appear in the final data is authenticated as ancient. The most generally accepted and widely applied authenticity for ancient DNA studies is to test for elevated deaminated cytosine residues towards the termini of the molecules: DNA damage. To date, this has primarily been used for single organisms and recently for read assemblies, however, these methods are not applicable for estimating DNA damage for ancient metagenomes with tens and even hundreds of thousands of species.
- ²⁴ **2. Methods** We present metaDMG, a novel framework and toolkit that allows for the estimation,

quantification and visualization of postmortem damage for single reads, single genomes
26 and even metagenomic environmental DNA by utilizing the taxonomic branching structure.
It bypasses any need for initial classification, splitting reads by individual organisms, and
28 realignment. We have implemented a Bayesian approach that combines a modified
geometric damage profile with a beta-binomial model to fit the entire model to the
30 individual misincorporations at all taxonomic levels.

3. **Results** We evaluated the performance using both simulated and published environmental
32 DNA datasets and compared to existing methods when relevant. We find `metaDMG` to be an
order of magnitude faster than previous methods and more accurate – even for complex
34 metagenomes. Our simulations show that `metaDMG` can estimate DNA damage at taxonomic
levels down to 100 reads, that the estimated uncertainties decrease with increased number
36 of reads and that the estimates are more significant with increased number of C to T
misincorporations.

38 4. **Conclusion** `metaDMG` is a state-of-the-art program for aDNA damage estimation and allows
for the computation of nucleotide misincorporation, GC-content, and DNA fragmentation
40 for both simple and complex ancient genomic datasets, making it a complete package for
ancient DNA damage authentication.

42 **Keywords:** ancient DNA, DNA damage estimation, DNA damage, `metaDMG`, metagenomics.

44 1 | INTRODUCTION

Throughout the life of an organism it contaminates its environment with DNA, cells, or tissue, thus
46 leaving genetic traces behind. As the cell leaves its host, DNA repair mechanisms stops and the DNA
is subjected to intra and extra cellular enzymatic, chemical, and mechanical degradation, resulting
48 in fragmentation and molecular alterations that over time lead to the characteristics of ancient
DNA (Briggs et al., 2007; Dabney, Meyer, and Pääbo, 2013). Ancient DNA (aDNA) has been shown
50 to persist in a diverse variety of environmental contexts, e.g. within fossils such as bones, soft-
tissue, and hair, as well as in geological sediments, archaeological layers, ice-cores, permafrost soil
52 for hundreds of thousands of years (Valk et al., 2021; Zavala et al., 2021). Common for all is that
they have an accumulated amount of deaminated cytosines towards the termini of the DNA strand,

54 which, when amplified, results in misincorporations of thymines on the cytosines (Ginolhac et al.,
2011; Dabney, Meyer, and Pääbo, 2013).

56 Even though postmortem DNA damage (PMD) is characterized by the four Briggs parameters
(Briggs et al., 2007), they are rarely used directly for asserting “ancientness”. Researchers work-
58 ing with ancient DNA tend to simply use the empirical C→T on the first position of the fragment
together with other supporting summary statistic of the experiment (Jónsson et al., 2013). Quanti-
60 fying PMD have become standard for single individual sources like hair, bones, teeth and also ap-
plied to smaller subsets of species in ancient environmental metagenomes (Pedersen et al., 2016;
62 Murchie et al., 2021; Wang, Pedersen, et al., 2021; Zavala et al., 2021). While this is a relatively fast
process for single individuals it becomes increasingly demanding, iterative, and time consuming as
64 the samples and the diversity within increases, as in the case for metagenomes from ancient soil,
sediments, dental calculus, coprolites, and other ancient environmental sources. It has therefore
66 been practice to estimate damage for only the key taxa of interest in a metagenome, as metage-
nomic samples easily include tens of thousands of different taxonomic entities, which makes a
68 complete estimate across the metagenomes computationally intractable, if not an impossible task
(Pedersen et al., 2016). To overcome these limitations, we designed a toolkit called `metaDMG` (pro-
70 nounced metadamage) which allows for the rapid computation of various statistics relevant for the
quantification of PMD at read level, single genome level, and even metagenomic level by taking into
72 account the intricate branching structure of the taxonomy of the possible multiple alignments for
the single reads.

74 Our thorough analysis with both simulated and real data shows that `metaDMG` is both faster at
ancient DNA damage estimation and provides more accurate damage estimates. Furthermore, as
76 `metaDMG` is designed with the increasingly large datasets that are currently generated in the field
of ancient environmental DNA in mind, `metaDMG` is able to process complex metagenomes within
78 hours instead of days. At the same time, it outperforms standard tools that estimate DNA damage
for single genomes and samples with low complexity. Furthermore, it can compute a global dam-
80 age estimate for a metagenome as a whole. Lastly, `metaDMG` is compatible with the NCBI taxonomy
and use `ngsLCA` (Wang, T. S. Korneliussen, et al., 2022) to perform a lowest common ancestor (LCA)
82 classification of the aligned reads to get precise damage estimates at all taxonomic levels. It also
allows for custom taxonomies and thus also the use of metagenomic assembled genomes (MAGs)
84 as references.

This paper is organized as follows. In **section 2** we present our statistical models including two novel test statistics, D_{fit} and Z_{fit} . We quantify the performance of our test statistics using various simulation approaches in **section 3**. The results of these simulations is shown in **section 4** and finally, the method and results are discussed in **section 5**.

2 | METHODS & MATERIALS

To quantify ancient damage, one can either compute it on a per read level or across an entire taxa. A priori, the actual biochemical changes which characterizes post mortem damage in a single read cannot be directly observed, but by aligning each fragment and considering the observed difference between the reference and read, the possible PMD can be computed. We have (re)implemented the approach used in PMDtools (Skoglund et al., 2014) which allows for the extraction of single DNA reads which are estimated to contain PMD, see **Appendix 1**. This approach, will preferentially choose reads that has excess of C→T in the first positions and can not be used directly for asserting or quantifying to what degree a given library might contain damaged fragments. We have therefore developed a novel statistical method that aims to mitigate this caveat by using all reads or reads that aligns to specific taxa. First we will define the mismatch matrices in **subsection 2.1** followed by the lowest common ancestor method in **subsection 2.2**. The mismatch matrices can further be improved by multinomial regression, see **subsection 2.3**, however, this requires more data than what is usually available in metagenomic studies. As such, we present the beta-binomial damage model in **subsection 2.4** which aims to work even on extremely low-coverage data.

2.1 | Mismatch matrices/nucleotide misincorporation patterns

We seek to obtain the pattern or signal of damage across multiple reads by generating what is called the mismatch matrix or the nucleotide misincorporation matrix. This matrix represents the nucleotide substitution counts across reads and provides us with the position dependent mismatch matrices, $M(x)$, with x denoting the position in the read, starting from 1. At a specific position x , $M_{\text{ref} \rightarrow \text{obs}}(x)$ describes the number of nucleotides that was mapped to a reference base B_{ref} but was observed to be B_{obs} , where B is one of the four bases: A, C, G, T. The number of C→T transitions at the first position, e.g., is denoted as $M_{C \rightarrow T}(x = 1)$.

Alignments for a read can be discarded based on their mapping quality, and we also give the

114 user the possibility of filtering out specific nucleotides of the read if the base quality score fall below
115 some threshold. The quality scores could also be used as probabilistic weights, however, due to
116 the four-bin discretization of quality scores on modern day sequencing machines, we limit the use
117 of these to filtering.

118 2.2 | Lowest Common Ancestor and Mismatch matrices

For environmental DNA (eDNA) studies a competitive alignment approach is routinely applied.
119 Here all possible alignments for a given read are considered. Each read is mapped against a multi
120 species reference databases (e.g. nucleotide or RefSeq from NCBI or custom downloaded). A sin-
121 gle read might map to a highly conserved gene that is shared across higher taxonomic ranks such
122 as class or even domains. This read will not provide relevant information due to the generality,
123 whereas a read that maps solely to a single species, e.g. would be indicative of the read being well
124 classified. We limit the tabulation and construction of the mismatch matrices to the subset of reads
125 that are well classified.

For each read, we compute the lowest common ancestor using all alignments contained within
126 the user defined taxonomic threshold (species, genus or family) and tabulate the mismatches ma-
127 trices for each cycle (Wang, T. S. Korneliussen, et al., 2022). If none of the alignments pass the
128 filtering thresholds (excess similarity, mapping quality, etc.), the read is discarded. Depending on
129 the run mode, we allow for the construction of these mismatch matrices on three different levels.
130 Firstly, we can obtain a basic single global mismatch matrix which could be relevant in a standard
131 single genome aDNA study and similar to the tabulation used in mapDamage (Jónsson et al., 2013).
132 Secondly, we can obtain the per reference counts, or, finally, if a taxonomy database has been
133 supplied, we can build mismatch matrices at the species level and aggregate from leaf nodes to
134 the internal taxonomic ranks (genus, kingdom etc) towards the root. We will use the term “taxa”
135 to refer to either of these levels; i.e. a specific taxa can either refer to a specific LCA, a specific
136 reference, or all reads in a global estimate, depending on the run-mode.

When aggregating the mismatch matrices for the internal nodes in our taxonomic tree, two
137 different approaches can be taken. Either all alignments of the read will be counted, which we will
138 refer to as weight-type 0, or the counts will be normalized by the number of alignments of each
139 read; weight-type 1, which is the default.

2.3 | Regression Framework

144 The nucleotide misincorporation frequencies are routinely used as the basis for assessing whether
or not a given library is ancient by looking at the expected drop of C→T (or its complementary G→A)
146 frequencies as a function of the position of the reads. This signal is caused by a higher deamination
rate in the single-strand part of the damaged fragment than that in the double strand part. The
148 mismatch matrix is constructed based on the empirical observations and are subject to stochastic
noise. The effect of noise in the mismatch matrix can be limited by the use of the multinomial
150 regression model. We continue the work of Cabanski et al., 2012 to provide four different regres-
sion methods to stabilize the raw mismatch matrix across all combinations of reference bases,
152 observed bases, strands and positions, see [Appendix 2](#) for details, derivation and results. Given
enough sequencing data, this approach will provide an improved, noise-reduced mismatch ma-
154 trix which would be relevant for single genome ancient DNA studies. However, for extremely low
coverage studies, such as environmental DNA, the method is likely to overfit and would not be as
156 suitable as the simplified model described in the [subsection 2.4](#).

2.4 | Damage Estimation

158 In standard ancient DNA context it is generally not possible to obtain vast amounts of data and
thus we propose two novel tests statistics, D_{fit} and Z_{fit} , that are especially suited for this common
160 scenario. The damage pattern observed in aDNA has several features which are well characterized.
By modelling these, one can construct observables sensitive to aDNA signal. We model the damage
162 patterns seen in ancient DNA by looking exclusively at the C→T transitions in the forward direction
(5') and the G→A transitions in the reverse direction (3'). For each taxa, we denote the number of
164 transitions, $k(x)$, as:

$$k(x) = \begin{cases} M_{C \rightarrow T}(x) & \text{for } x > 0 \quad (\text{forward}) \\ M_{G \rightarrow A}(x) & \text{for } x < 0 \quad (\text{reverse}), \end{cases} \quad (1)$$

166

and the number of reference counts $N(x)$:

$$N(x) = \begin{cases} \sum_{i \in \{A,C,G,T\}} M_{C \rightarrow i}(x) & \text{for } x > 0 \quad (\text{forward}) \\ \sum_{i \in \{A,C,G,T\}} M_{G \rightarrow i}(x) & \text{for } x < 0 \quad (\text{reverse}). \end{cases} \quad (2)$$

170

The damage frequency is thus $f(x) = k(x)/N(x)$.

A natural choice of likelihood model would be the binomial distribution. However, we found

172 that a binomial likelihood lacks the flexibility needed to deal with the large amount of variance
(overdispersion) we found in the data due to poorly curated references and possible misalignments.

174 To accommodate overdispersion, we instead apply a beta-binomial distribution, $\mathcal{P}_{\text{BetaBinomial}}$, which
treats the probability of deamination, p , as a random variable following a beta distribution¹ with
176 mean μ and concentration ϕ : $p \sim \text{Beta}(\mu, \phi)$. The beta-binomial distribution has the following
probability density function:

$$\mathcal{P}_{\text{BetaBinomial}}(k | N, \mu, \phi) = \binom{N}{k} \frac{B(k + \mu\phi, N - k + \phi(1 - \mu))}{B(\mu\phi, \phi(1 - \mu))}, \quad (3)$$

¹ Note that we do not parameterize the beta distribution in terms of the common (α, β) parameterization, but instead using the more intuitive (μ, ϕ) parameterization. One can re-

parameterize $(\alpha, \beta) \rightarrow (\mu, \phi)$ using the following two equa-

tions: $\mu = \frac{\alpha}{\alpha+\beta}$ and $\phi = \alpha + \beta$

(Cepeda-Cuervo and Cifuentes-

Amado, 2017).

180 where B is defined as the beta function:

$$B(x, y) = \frac{\Gamma(x)\Gamma(y)}{\Gamma(x+y)}, \quad (4)$$

with $\Gamma(\cdot)$ being the gamma function (Cepeda-Cuervo and Cifuentes-Amado, 2017).

184 The close resemblance to a binomial model is most easily seen by comparing the mean and
variance of a random variable k following a beta-binomial distribution, $k \sim \mathcal{P}_{\text{BetaBinomial}}(N, \mu, \phi)$:

$$\mathbb{E}[k] = N\mu \quad (5)$$

186

$$\mathbb{V}[k] = N\mu(1 - \mu) \frac{\phi + N}{\phi + 1}.$$

The expected value of k is similar to that of a binomial distribution and the variance of the beta-
188 binomial distribution reduces to a binomial distribution as $\phi \rightarrow \infty$. The beta-binomial distribution
can thus be seen as a generalization of the binomial distribution.

190 Note that both equation (3) and (5) relate to the damage at a specific base position (cycle),
i.e. for a single k and N . To estimate the overall damage in the entire read using the position
192 dependent counts, $k(x)$ and $N(x)$, we model μ as being position dependent, $\mu(x)$, and assume a
position-independent concentration, ϕ . We model the damage frequency with a modified geomet-
194 ric sequence, i.e. exponentially decreasing for discrete values of x :

$$y(x; A, q, c) = A(1 - q)^{|x|-1} + c. \quad (6)$$

196 Here A is the amplitude of the damage and q is the relative decrease of damage pr. position. A
background, c , was added to reflect the fact that the mismatch between the read and reference
198 might be due to other factors than just ancient damage. As such, we allow for a non-zero amount
of damage, even as $x \rightarrow \infty$. This is visualized in **Figure 1** along with a comparison between the
200 classical binomial model and the beta-binomial model.

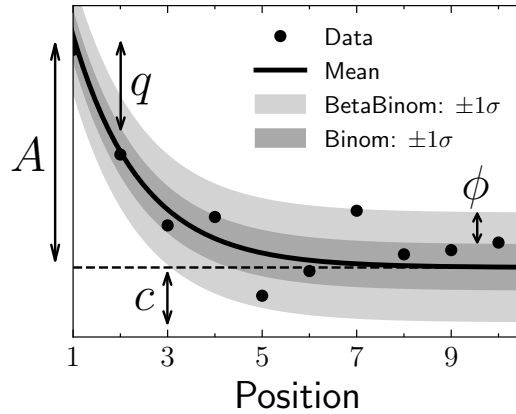


Figure 1. Illustration of the damage model. The figure shows data points as circles and the damage, $f(x)$, as a solid line. The amplitude of the damage is A , the offset is c , and the relative decrease in damage pr. position is given by q . The damage uncertainty for a binomial model is shown in dark grey and the uncertainty for a beta-binomial model in light grey.

²⁰² To estimate the four fit parameters, A , q , c , and ϕ , we apply Bayesian inference to utilize domain specific knowledge in the form of priors. We assume weakly informative beta-priors² for both A , q , and c . In addition to this, we assume an exponential prior on ϕ with the requirement of $\phi > 2$ to avoid too much focus on 0-or-1 probabilities (McElreath, 2020). The final model is thus:

$$\begin{aligned}
 \text{[206] } [A \text{ prior}] \quad A &\sim \text{Beta}(0.1, 10) \\
 \text{[q prior]} \quad q &\sim \text{Beta}(0.2, 5) \\
 \text{[208] } [c \text{ prior}] \quad c &\sim \text{Beta}(0.1, 10) \\
 \text{[phi prior]} \quad \phi &\sim 2 + \text{Exponential}(1/1000) \\
 \text{[210] } [\text{likelihood}] \quad k_i &\sim \mathcal{P}_{\text{BetaBinomial}}(N_i, y(x_i; A, q, c), \phi),
 \end{aligned} \tag{7}$$

²¹² where i is an index running over all positions.

We define the damage due to deamination, D , as the background-subtracted damage frequency at the first position: $D \equiv y(x = \pm 1) - c$. As such, D is the damage related to ancientness. Using the properties of the beta-binomial distribution, eq. (5), we find the mean and variance of D :

$$\begin{aligned}
 \mathbb{E}[D] &\equiv D_{\text{fit}} = A \\
 \text{[216] } \mathbb{V}[D] &\equiv \sigma_D^2 = \frac{A(1-A)}{N} \frac{\phi + N}{\phi + 1}.
 \end{aligned} \tag{8}$$

Since D estimates the overexpression of damage due to ancientness, not only is the mean of D , D_{fit} , relevant but also the certainty of it being non-zero (and positive). We quantify this through the

significance $Z_{\text{fit}} = D_{\text{fit}}/\sigma_D$ which is thus the number of standard deviations ("sigmas") away from zero. Assuming a Gaussian distribution of D , $Z_{\text{fit}} > 2$ would indicate a probability of D being larger than zero, i.e. containing ancient damage, with more than 97.7% probability. This assumption works well in the case of many reads or a high amount of damage due to central limit theorem. When the assumption breaks down, the significance is still a relevant test statistic, it is only the conversion to a probability that will become biased.

These two values allows us to not only quantify the amount of ancient damage (D_{fit}) but also the certainty of this damage (Z_{fit}) without having to run multiple models and comparing these. An intuitive interpretation of our D_{fit} statistic is, that this is the excess deamination in the beginning of the read, taking all cycle positions into account and excluding the constant deamination background (c). This is visually similar to the A parameter in [Figure 1](#).

We perform the Bayesian inference of the parameters models using Hamiltonian Monte Carlo (HMC) sampling which is a particular of Monte Carlo Markov Chain (MCMC) algorithm (Betancourt, 2018). Specifically, we use the NUTS implementation in NumPyro (Phan, Pradhan, and Jankowiak, 2019), a Python package which uses JAX (Bradbury et al., 2018) under the hood for automatic differentiation and JIT compilation. We treat each taxa as being independent and generate 1000 MCMC samples after an initial 500 samples as warm up.

Since running the full Bayesian model is computationally expensive, we also allow for a faster, approximate method by fitting the maximum a posteriori probability (MAP) estimate. We use iMInuit (Dembinski et al., 2021) for the MAP optimization with Numba acceleration (Lam, Pitrou, and Seibert, 2015) for even faster run times. On a Macbook M1 Pro model from 2021, the timings for running the full Bayesian model is 1.41 ± 0.04 s pr. fit and for the MAP it is 4.34 ± 0.07 ms pr. fit, showing more than a 2 order increase in performance (around 300x) for the approximate model. Both models allow for easy parallelisation to decrease the computation time.

2.5 | Visualisation

We provide an interactive graphical user interface (dashboard) to visualise, explore, and manipulate the results from the modelling phase. An interactive example of this can be found online (<https://metadmg.onrender.com/>). The structure of the dashboard is explained in [Figure 2](#). The dashboard allows for filtering, styling and variable selection, visualizing the mismatch matrix related to a specific taxa, and exporting of both fit results and plots. By filtering, we include both filtering by

sample, by the summary statistics of the data (e.g. requiring D_{fit} to be above a certain threshold),
250 and even by taxonomic level (e.g. only looking at taxa that are part of the Mammalia class). We
greatly believe that a visual overview of the fit results increase understanding of the data at hand.
252 The dashboard is implemented with Plotly plots and incorporated into a Dash dashboard (Plotly,
2015).

254 3 | SIMULATION STUDY

To determine metaDMG's performance, we performed a set of rigorous in-silica simulations to identify
256 and quantify any possible biases as well the accuracy of our test statistics. Overall, the simulations
can be split two groups. The first is based on a genome from a single species and is used to mea-
258 sure the performance of the actual damage estimation and damage model. The second is based
on synthetic ancient metagenomic datasets using the statistics and nature of a set of published
260 ancient metagenomes.

3.1 | Single-genome simulations

262 The first simulations follow a simple setup in which we extract reads from a set of representa-
tive genomes having variable length and GC-content. We next added post-mortem damage mis-
264 incorporations using NGSNGS (Henriksen, Zhao, and T. Korneliussen, 2022) a recent implemen-
tation of the original Briggs model similar to Gargammel (Neukamm, Peltzer, and Nieselt, 2021)
266 and lastly added sequencing errors (Renaud et al., 2017). All reads are hereafter mapped using
Bowtie2 against each of the respective reference genomes and ancient DNA damage estimated
268 the DNA damage using metaDMG. The simulations were computed with varying amount of damage
added by changing the single-stranded DNA deamination, δ_{SS} in the original Briggs model (Briggs
270 et al., 2007).

³ NCBI: NC_012920.1

⁴ NCBI: KX703002.1

⁵ NCBI: NZ_CP024731.1

⁶ NCBI: NZ_LS483369.1

⁷ NCBI: GCA_001929375.1

In detail, we focused on the following genomes; *Homo Sapiens* mitochondrial³, a *Betula nana*
272 chloroplast⁴, and three microbial genomes (*Fusobacterium pseudoperiodonticum*⁵, *Neisseria cinerea*⁶,
and *Actinomyces oris* strain S64C⁷) with the varying GC-content, low (28%), medium (37%), and high
274 (50%) respectively. For each simulation, we performed 100 independent replications to measure
the variability of the parameter estimation and quantify the robustness of the estimates. We fur-
276 ther simulated eight different sets of damage (0%, 1%, 2%, 5%, 10%, 15%, 20%, and 30% damage
on position 1), all with 13 sets of different number of reads (10, 25, 50, 100, 250, 500, 1.000, 2.500,

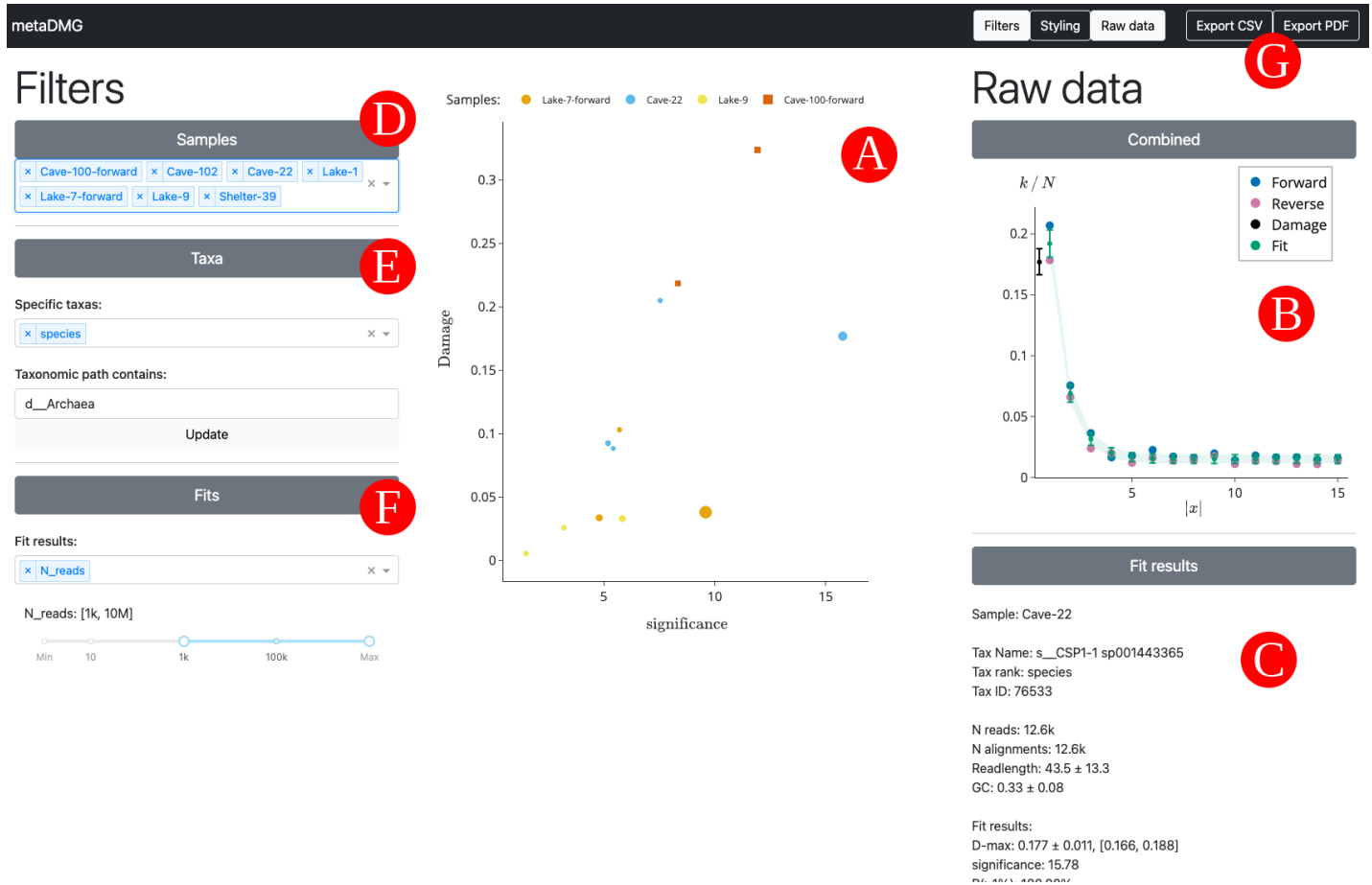


Figure 2. Overview of the interactive metaDMG dashboard. A) The main damage plot shows the damage (D_{fit}) on the y-axis and the significance (Z_{fit}) on the x-axis. Each point is a single taxa from one of the metagenomic samples, see *Table 1*. Once clicked on a specific taxa, the right-hand window shows information about the selected taxa and related fit. B) The top window shows a plot of the damage frequency for both the forward and reverse direction along with the estimated fit and damage. C) Below, the results of the fit are shown, including taxonomic information, read-specific information, the fit results, and the full taxonomic path. D) In the left filtering window, the samples to include can be selected. E) This windows allows for selection based on taxa-specific criteria. Here we show a selection of only taxa with “species” as their LCA and taxa that are part of the archaea domain. F) The final filtering window allows for setting fit related thresholds such as the minimum damage or significance. Here it is shown discarding taxa with fewer than 1000 reads. G) In the top right, after the selection and filtering process is finished, the final taxa can be exported to a CSV file along with all of the fit information, or the damage plots can be generated and saved.

278 5.000, 10.000, 25.000, 50.000, and 100.000 reads). We also sought to measure the effect of the
280 fragment lengths using three sets of different fragment length distributions sampled from a *log-normal*
282 distribution with mean 35, 60, and 90, each with a standard deviation of 10). Furthermore,
284 to investigate whether the damage estimation by metaDMG is independent of contig size, we artificially
286 created three different genomes by sampling 1.000, 10.000 or 100.000 different basepairs from a uniform categorical distribution of A, C, G, and T. Based on these three genomes, we added
artificial deamination for a different number of reads, as for the other simulations. Lastly, we also
created 1000 repetitions of non-damaged simulations for *Homo Sapiens* to measure the rate of
false positives. The exact commands used can be found in [Appendix 3](#).

To compare the damage estimates to known values, for each of the genomes mentioned above
288 and for each amount of artificial damage, we generated 1.000.000 reads using NGSNGS without
any added sequencing noise. The values we compare is the difference in damage frequency at
290 position 1 and 15:

$$D_{\text{known}} = \frac{f(x=1) - f(x=15)}{2} + \frac{f(x=-1) - f(x=-15)}{2}, \quad (9)$$

292 which is the average of the C→T damage frequency difference and the G→A damage frequency
difference.

294 3.2 | Metagenomic Simulations

A metagenome contains a complex mixture of organisms, all with highly different characteristics
296 in GC content, read length, abundance, or degree of DNA damage, and there are large differences
between different environments. It is therefore far from simple to obtain DNA damage estimates
298 for such multitude of organisms. In order to test the accuracy and sensitivity of metaDMG, we simulated
six of the nine ancient metagenomes (with more than 1 million reads) covering a wide span
300 of environments and ages ([Table 1](#)).

First, we mapped all reads of each metagenome with bowtie2 against a database consisting of
302 the GTDB (r202) (Parks et al., 2018) species cluster reference sequences, all organelles from NCBI
RefSeq (NCBI Resource Coordinators, 2018), and the reference sequences from CheckV (Nayfach et
304 al., 2021). We then used bam-filter v1.0.11 (Fernandez-Guerra, 2022a) with the flag --read-length-freqs
to get read length distributions for each genome reads aligned to and their respective abundance.
306 Next, we filtered genomes with an observed-to-expected coverage ratio greater than 0.75 using

Table 1. Metagenomic samples. “Name” is the name of the sample used throughout this paper. “Site” is the type of metagenomic site. “Type” is the type of environment. “Age” is the approximate age of the sample in kyr Bp. “Sediment” is the name type of sediment. “Instrument” is the Illumina model. “Library” is the library type where D. means double stranded and S. means single stranded. “Reads” is the raw number of reads (in millions). “Source” is the source of the data. The dagger (†) indicates samples that were not a part of the metagenomic simulation pipeline.

Name	Site	Type	Age (kyr)	Sediment	Instrument	Library	Reads (M)	Source
Library-0 [†]	Control	Control	0	Reagents	HiSeq4000	D.	19.7	(Ardelean et al., 2020)
Pitch-6	Syltholmen pitch	Chewed organic material	5.7	Organic material	HiSeq2500	D.	150.3	(Jensen et al., 2019)
Lake-1 [†]	Spring Lake	Lake gyttja/sediment	1.4	Organic material	HiSeq 100	D.	49.8	(Pedersen et al., 2016)
Lake-7	Lake CH12	Lake gyttja/sediment	6.7	Organic material	HiSeq2500	S.	291.9	(Schulte et al., 2021)
Lake-9	Spring Lake	Lake gyttja/sediment	9.2	Organic material	HiSeq 100	D.	128.4	(Pedersen et al., 2016)
Shelter-39 [†]	Abri Pataud	Rock shelter	39.4	Sediment	MiSeq	S.	0.4	(Braadbaart et al., 2020)
Cave-22	Chiquihuite cave	Cave sediment	22.2	Carbonate rock	HiSeq4000	D.	5.7	(Ardelean et al., 2020)
Cave-100	Eustatas Cave	Cave sediment	100	Carbonate rock	HiSeq2500	S.	21.8	(Vernot et al., 2021)
Cave-102	Pesturina Cave	Neanderthal tooth	102	Dental calculus	HiSeq4000	D.	12.3	(Fellows Yates et al., 2021)

bamfilter. The filtered BAM files were then processed by metaDMG to obtain misincorporation matrices for each genome. The abundance tables, fragment length distribution, and misincorporation matrices were then used in aMGSIM-smk v0.0.1 (Fernandez-Guerra, 2022b), a Snakemake workflow (Mölder et al., 2021) that facilitates the generation of multiple synthetic ancient metagenomes. The underlying tools in this workflow is the gargamel toolkit (Renaud et al., 2017), that based on input read length distribution extract a subset of sequences (FragSim) with similar length. This is then followed by the addition of $C \rightarrow T$ substitutions (DeamSim) which mimics the postmortem damage process. Finally the deaminated sequences are passed to the ART (Huang et al., 2012) for sequence simulation. The data used and generated by the workflow can be obtained from ERDA. We then performed taxonomic profiling and damage estimation using identical parameters as for the synthetic reads generated by aMGSIM-smk.

318 4 | RESULTS

We tested the accuracy and performance of the metaDMG damage estimates, D_{fit} , using a set of different simulation scenarios and subsequently tested on 9 real-life ancient metagenomic dataset.

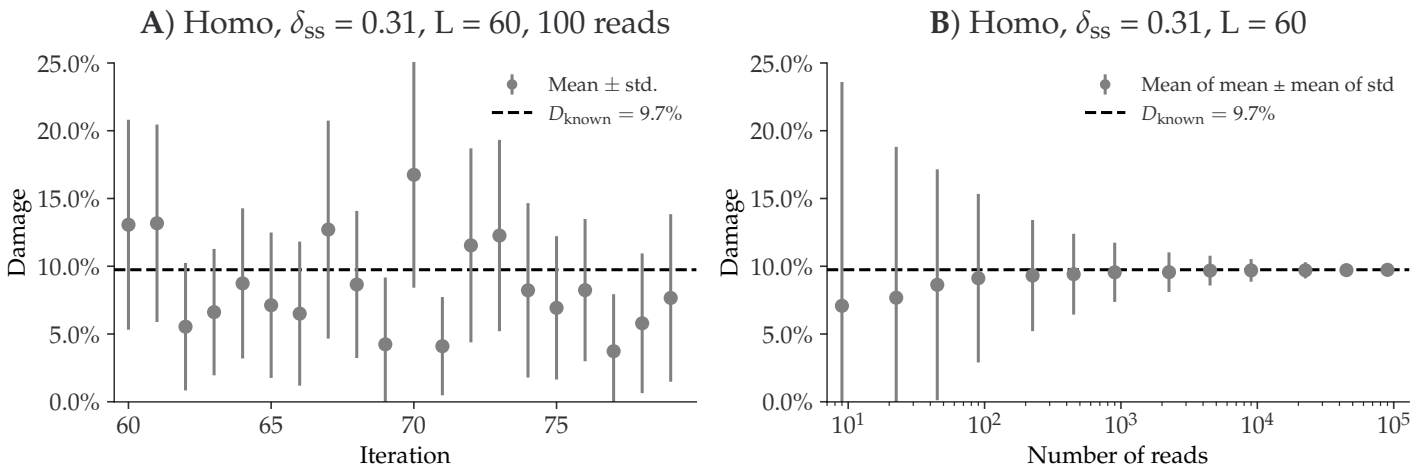


Figure 3. Overview of the single-genome simulations based on the Homo Sapiens genome with a fragment length distribution with mean 60 and the Briggs parameter $\delta_{SS} = 0.31$ (approximately 10% damage). **A)** This plot shows the estimated damage (D_{fit}) of 20 replicates, each with 100 reads. The grey points show the mean damage (with its standard deviation as errorbars). The known damage (D_{known}) is shown as a dashed line, see eq. (9). **B)** This plot shows the average damage as a function of the number of reads. The grey points show the average of the individual means (with the average of the standard deviations as errors).

4.1 | Single-genome simulation results

322 To illustrate the results the performance on single-genomes, we first focus on a single, specific set
 323 of simulation parameters. This simulation is based on the Homo Sapiens genome with the Briggs
 324 parameter $\delta_{SS} = 0.31$ (approximately 10% damage) and a mean fragment length of 60. In general,
 325 we use $\delta = 0.0097$, $\nu = 0.024$, and $\lambda = 0.36$ as Briggs parameters, while varying δ_{SS} (Briggs et al.,
 326 2007). We show the metaDMG damage results for the 100 independent replications in **Figure 3**. The
 327 left part of the figure shows the individual metaDMG damage estimates for an arbitrary choice of 20
 328 replications (iteration 60 to 79). When the damage estimates are very low, the distribution of D_{fit} is
 329 skewed (restricted to positive values), sometimes leading to errorbars going into negative damage,
 330 which represents unrealistic estimates. The right hand side of the figure visualizes the average
 331 amount of damage based on all 100 replications across a varying number of reads. This shows
 332 that the damage estimates converge to the known value with more data, and that one needs more
 333 than 100 reads to even get strictly positive damage estimates (when including uncertainties) for
 334 this specific set of simulation parameters.

Across multiple simulations, each with 8 different damage levels, 13 different numbers of reads,
 335 and 100 replications, we find no significant difference in test statistic across different species (**Fig-**

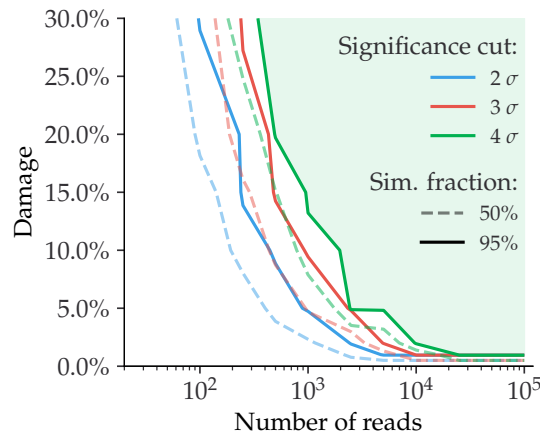


Figure 4. Relationship between the damage and the number of reads for simulated data (single-genome).

Given a specific significance cut, the solid contour line shows the relationship between the amount of damage and the number of reads required to be able to correctly infer damage in 95% of the taxa. The dashed line shows the similar value for a simulation fraction of 50%. The green part of the figure shows the “good” region of number of reads and estimated damage, given than one wants to be more than 95% certain of correctly identifying damage with more than 4σ confidence.

ure S5 and Figure S6), across different GC-levels (Figure S7–Figure S9), different fragment length
 338 distributions (Figure S10–Figure S12), or even different contig lengths (Figure S13–Figure S15), see
Appendix 4. Based on the single-genome simulations, we compute the relationship between the
 340 amount of damage in a taxa and the number of reads required to correctly infer that the reads
 from that taxa are damaged, see **Figure 4**. If we want to assert damage with a significance of more
 342 than 2 (solid blue line) in a sample with around 5% expected damage, it requires about 1000 reads
 to be 95% certain that we will find results this good, whereas we only need 100 reads if our target
 344 organism has 30 % damage.

Finally, to quantify the risk of incorrectly classifying a non-ancient taxa as damaged, we created
 346 1000 independent replications for a varying number of reads, where none of them had any artificial
 ancient damage applied, only sequencing noise. **Figure 5** shows the damage (D_{fit}) as a function of
 348 the significance (Z_{fit}) for the case of 1000 reads. Even though the estimated damage is larger than
 zero, the damage is non-significant since the significance is less than one. When looking at all the
 350 figures across the different number of reads, see **Appendix 5**, we note that a relaxed significance
 threshold requiring that $D_{\text{fit}} > 1\%$ and $Z_{\text{fit}} > 2$ would filter out all of non-damaged points. Overall
 352 the conclusion being that our novel test statistic is conservative and has low false positive rate.

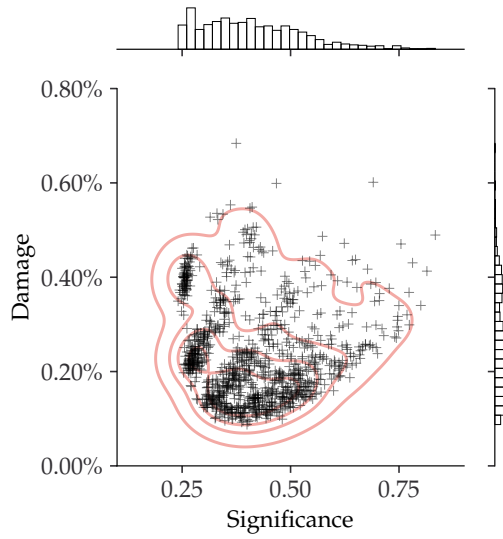


Figure 5. Inferred damage of modern, simulated data (single-genome). The plot shows the inferred damage estimates of 1000 replicates, each with 1000 reads and no artificial ancient damage applied. Each single cross corresponds to a simulation and the red lines outlines the kernel density estimate (KDE) of the damage estimates. The marginal distributions are shown as histograms next to the scatter plot.

4.2 | Metagenomic simulation results

With the full metagenomic simulation pipeline we can further probe the performance of `metaDMG`. By considering the different metagenomic scenarios, see *Table 1*, at different steps in the pipeline, we are able to show that `metaDMG` provides relevant and accurate damage estimates.

To verify that the risk of getting false positives is non-significant, we run `metaDMG` on the metagenomic assemblages after fragmentation with `FragSim`, but before any deamination with `DeamSim` has yet been added. We find that the previously established relaxed significance threshold ($D_{\text{fit}} > 1\%$ and $Z_{\text{fit}} > 2$) correctly filters out all of the taxa, see *Figure 6*. This is as expected, as there has not yet been added any artificial post mortem damage in the form of deamination.

We see a clear difference in the damage estimates between the ancient and the non-ancient taxa once we add deamination with `DeamSim` and sequencing errors with `ART`, see *Figure 7*. The non-ancient taxa would still not pass the relaxed threshold, in contrast to the taxa in the ancient samples.

The results of *Figure 7* are summarized in *Table 2*. We find that Cave-100-forward, Cave-102, Pitch-6 all have more than 60% of their ancient taxa correctly labelled as damaged according to the relaxed threshold, while it for Cave-22 and Lake-7-forward is a bit lower and Lake-9 does not show

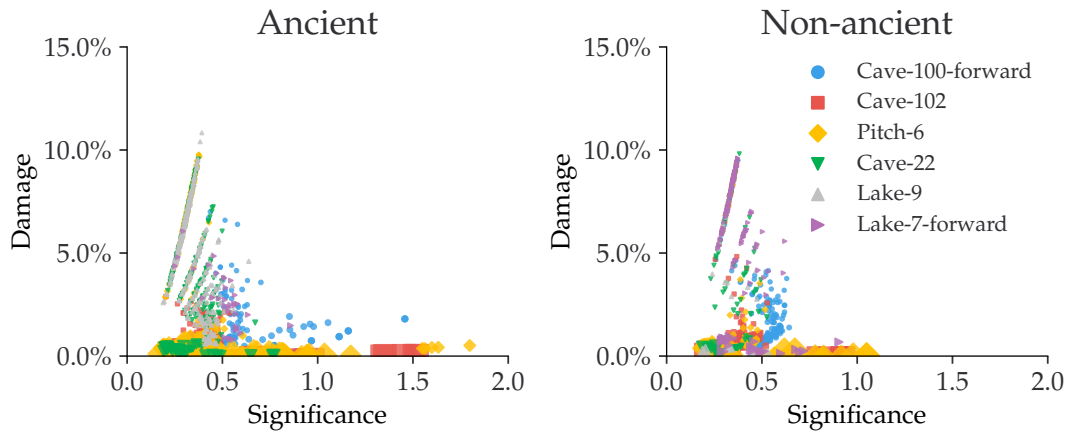


Figure 6. Estimated amount of damage as a function of significance for metagenomic simulations. This figure shows the metagenomic simulations after FragSim has been applied, but before including any deamination or sequencing errors. We generate both non-ancient and ancient taxa in the simulation pipeline. The left subfigure shows the damage of the ancient taxa and similarly for the non-ancient taxa in the right subfigure.

any clear support of damage. However, once we condition on the requirement of having more than
 370 100 reads, the fraction of ancient taxa correctly identified as ancient increases to more than 90%
 for most of the samples. A small investigation of one of the ancient taxa (*Stenotrophomonas Mal-*
 372 *tophilia*) in the simulation that did not meet the criteria to be ancient metaDMG, i.e. a false negative,
 can be found in [Appendix 6](#).

374 4.3 | Real Data

The results from running the real metagenomic data through the metaDMG pipeline show clear ev-
 376 idence of taxa with significant DNA damage present in the metagenome and a layered pattern
 similar to what was observed in the simulated ancient metagenomes, see [Figure 8](#).

378 As DNA damage is not a function of time, we cannot expect that there is a direct relation be-
 between damage and time, however, we do see that the oldest samples, Cave-100 and Cave-102, see
 380 [Table 1](#), which are 100 and 102 thousand years BP, show the highest amount of damage of all the
 metagenomes. Both the Pitch-6 and Cave-22 samples, which are 6 and 22 thousand year old and
 382 thus younger than two above mentioned cave samples, have almost similar levels of damage. This
 is not unexpected as the micro environment surrounding the layer in which the metagenome was
 384 found plays a significant role in the state of DNA. In our case, the younger Pitch-6 derives from a
 water logged but open air site, while the Cave-22 sample was obtained in dry but cool (~11 degree
 386 Celsius year around) cave layers.

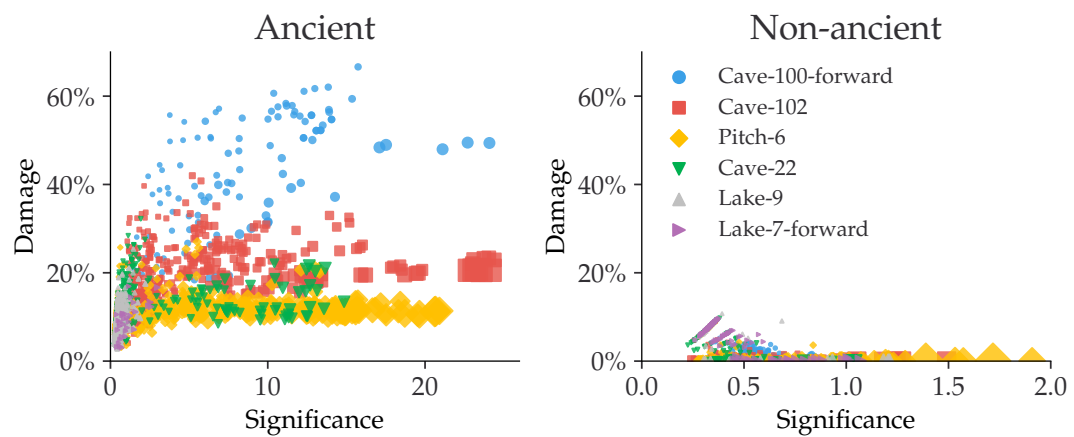


Figure 7. Estimated amount of damage as a function of significance for metagenomic simulations. This figure shows the metagenomic simulations after fragmentation, deamination, and sequencing errors have been applied. The left subfigure shows the damage of the ancient taxa and similarly for the non-ancient taxa in the right subfigure.

Table 2. metaDMG damage results for the six different metagenomic simulations. The first column is the total number of taxa, the second column is the total number of taxa that would pass the threshold of $D_{fit} > 1\%$ and $Z_{fit} > 2$, the third column is the number of taxa with more than 100 reads, and the final column is the number of taxa with more than 100 reads that also do pass the cut.

Sample	Total	Pass	+100 Reads	+100 Reads and Pass		
Cave-100-forward	135	107	79.3%	88	87	98.9%
Cave-102	500	326	65.2%	309	285	92.2%
Pitch-6	415	260	62.7%	274	260	94.9%
Cave-22	393	71	18.1%	73	69	94.5%
Lake-9	410	2	0.5%	8	0	0%
Lake-7-forward	32	4	12.5%	6	4	66.7%

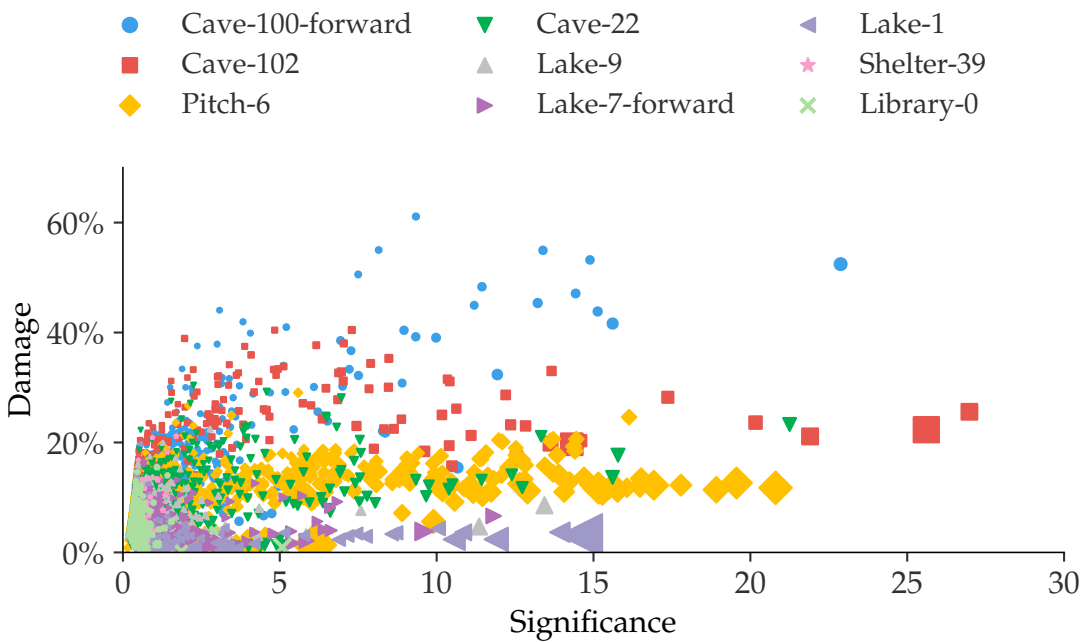


Figure 8. Estimated amount of damage as a function of significance using the real data, see *Table 1*.

The metagenomes with the least DNA damage are the ones from the lake sediments (Lake-1, 388 Lake-7 and Lake-9). These samples do show some taxa with significant DNA damage, although they do not have a strong damage signal.

390 Importantly, we find that in the true metagenomes, metaDMG is able to assign low significance to the taxa that likely are not damaged or that have too little data, see e.g. the upper right hand corner 392 of *Figure 9*. This subfigure shows the damage plot for the *Gallus Gallus* species (red junglefowl) 394 from the Lake-1 sample. This particular species only has $D_{\text{fit}} = 2.2\%$ and $Z_{\text{fit}} = 1.0$, which does 396 not satisfy the relaxed DNA damage threshold ($D_{\text{fit}} > 1\%$, $Z_{\text{fit}} > 2$). In addition to the *Gallus Gallus* species, *Figure 9* further shows examples of species with large amounts of data (*Homo Sapiens* in 398 the Pitch-6 sample and *Crocuta Crocuta* in the Cave-100 sample, based only on forward data), and 400 an example of medium damage (*Equisetum Arvense* in Lake-7, based only on forward data).

402 Interestingly, and of high importance for downstream interpretation, is that for certain samples, some taxa were found to have a high significance although with lower DNA damage than what is 404 observed across the given metagenome as a whole. This underlines the need to evaluate the DNA 406 damage variation within each metagenome, perform a proper outlier test and the basic setting of 408 logical thresholds.

We find that when using the relaxed DNA damage threshold, metaDMG falsely classifies a single

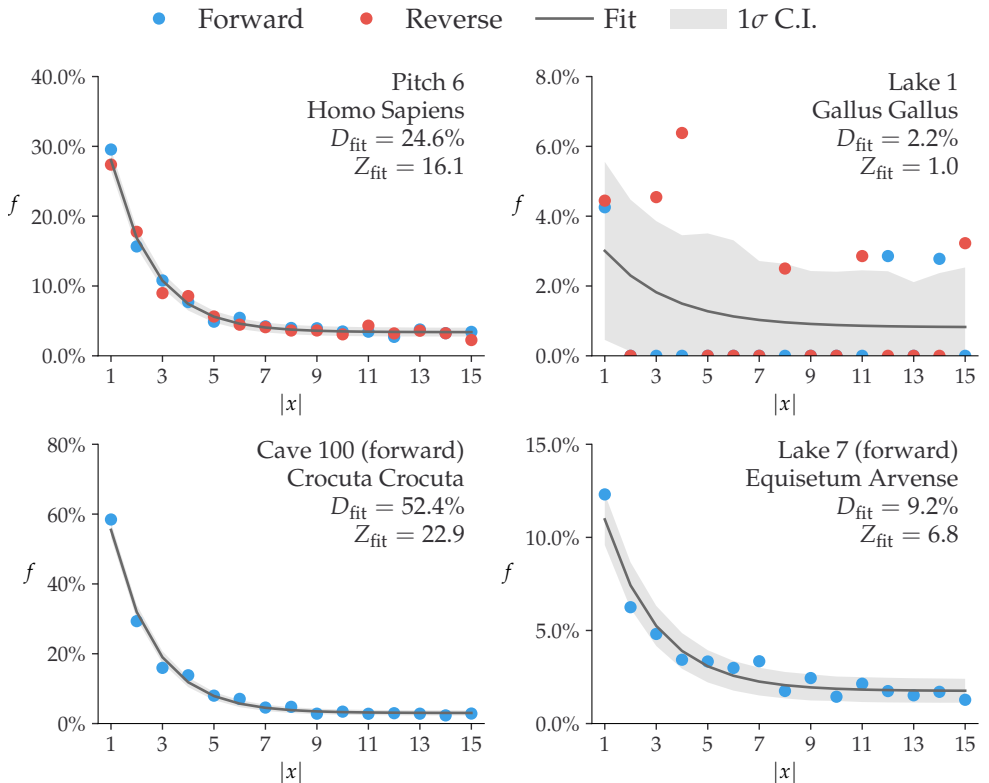


Figure 9. Damage plots of four representative species from the real-data metagenomic samples, see *Table 1*.

Each subfigure shows the damage rate $f(x) = k(x)/N(x)$ as a function of position x for both forward ($C \rightarrow T$) and reverse ($G \rightarrow A$). The metaDMG fit is shown in grey with the 68% credible intervals as shaded regions. In the upper right corner of each subfigure, the information about the sample and the species together with the metaDMG damage estimates is shown.

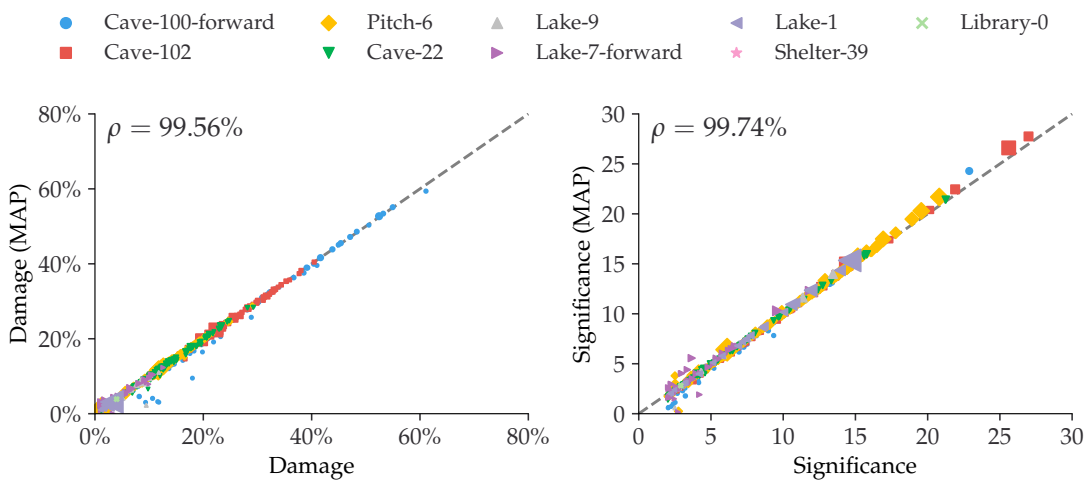


Figure 10. Comparison between the full Bayesian model and the fast, approximate, MAP model for the estimated damage and significance. The figure shows data after a loose cut of $D_{\text{fit}} > 1\%$, $Z_{\text{fit}} > 2$ and more than 100 reads. The dashed, grey line shows the 1:1 ratio and the correlation, ρ , is shown in the upper left corner.

404 of the taxa from the control test Library-0 as being ancient. However, with a more conservative
 405 damage threshold ($D_{\text{fit}} > 2\%$, $Z_{\text{fit}} > 3$, more than 100 reads), none of the taxa from the library
 406 control are classified as ancient.

4.4 | Bayesian vs. MAP

408 Due to the higher computational burden of computing the full Bayesian model compared to the
 409 faster, approximate MAP model in samples with several thousand taxa, the MAP model is in prac-
 410 tice the model of choice due to lower computational complexity. We compared the performance
 411 of D_{fit} and Z_{fit} on the real datasets in *Table 1*, see *Figure 10*. This figure compares the estimated
 412 damage between the Bayesian model and the MAP model (left subfigure) and the estimated sig-
 413 nificances (right subfigure) for taxa passing a threshold of $D_{\text{fit}} > 1\%$, $Z_{\text{fit}} > 2$, and more than 100
 414 reads. The figure shows that the vast majority of taxa map 1:1 between the Bayesian and the MAP
 415 model. It should be noticed that the taxa with the worst correspondence in damage estimates
 416 are all based on forward-only fits, i.e. with no information from the reverse strand, which leads
 417 to less data to base the fits on. For the comparison with no thresholds applied, see *Figure S23* in
 418 *Appendix 7*. We recommend to use the full, Bayesian model in the case of extremely low-coverage
 419 data or when used on only a small number of taxa (e.g. when using `metaDMG` in global-mode).

420 4.5 | Existing Methods

To our knowledge there are not currently available methods for assessing and quantifying post-
422 mortem DNA damage in a metagenomic context. We compare the performance of the D_{fit} statistic
in `metaDMG` to existing methods such as those found in PyDamage (Borry et al., 2021). Since PyDam-
424 age is based solely on single genome analysis we use the non-LCA mode of `metaDMG`. This mode
iterates through the different referenceIDs for all mapped reads and estimates the damage for
426 each. In general, we find that `metaDMG` is more conservative, accurate and precise in its damage
estimates.

428 One example of this can be found in *Figure 11*, which shows both the `metaDMG` and PyDamage
results of the simulations described in *subsection 3.1*, in particular the 100 replications of the Homo
430 Sapiens single-genome with 100 reads and 15% added artificial damage (and a fragment length
distribution with mean 60). *Figure 11* shows that the `metaDMG` estimates are between 5% and 25%
432 damage, while PyDamage estimates up to more than 50% damage, in a sample with 15% artificially
added damage. The comparisons between `metaDMG` and PyDamage for the other sets of simulation
434 parameters can be found in *Figure S24–Figure S31* in *Appendix 8*.

To compare the computational performance, we use the real-life Pitch-6 sample (i.e. non-
436 simulated), see *Table 1*. This alignment file (in BAM-format) takes up 857 MB of space and has
3.7 millions reads with a total of 19 million alignments to 11.433 unique taxa. When using only
438 a single core, PyDamage took 1105s to compute all fits, while `metaDMG` took 88s, a factor of 12.6x
faster. The rest of the timings are shown in *Table 3*. PyDamage requires the alignment files to
440 be sorted by chromosome position and be supplied with an index file, allowing it to iterate fast
through the alignment file, at the expense of computational load before running the actual dam-
442 age estimation. `metaDMG` on the other hand requires the reads to be sorted by name to minimize
the time it takes to run the LCA.

444 5 | DISCUSSION

To our knowledge there are no currently available methods other than `metaDMG` that is geared to-
446 wards damage analysis in a metagenomic setting. It is the first general framework designed specif-
ically for the quantification of ancient damage in all contexts. The toolkit contains various inter-
448 linked and independent modules including a state-of-the-art graphical user interface that allow

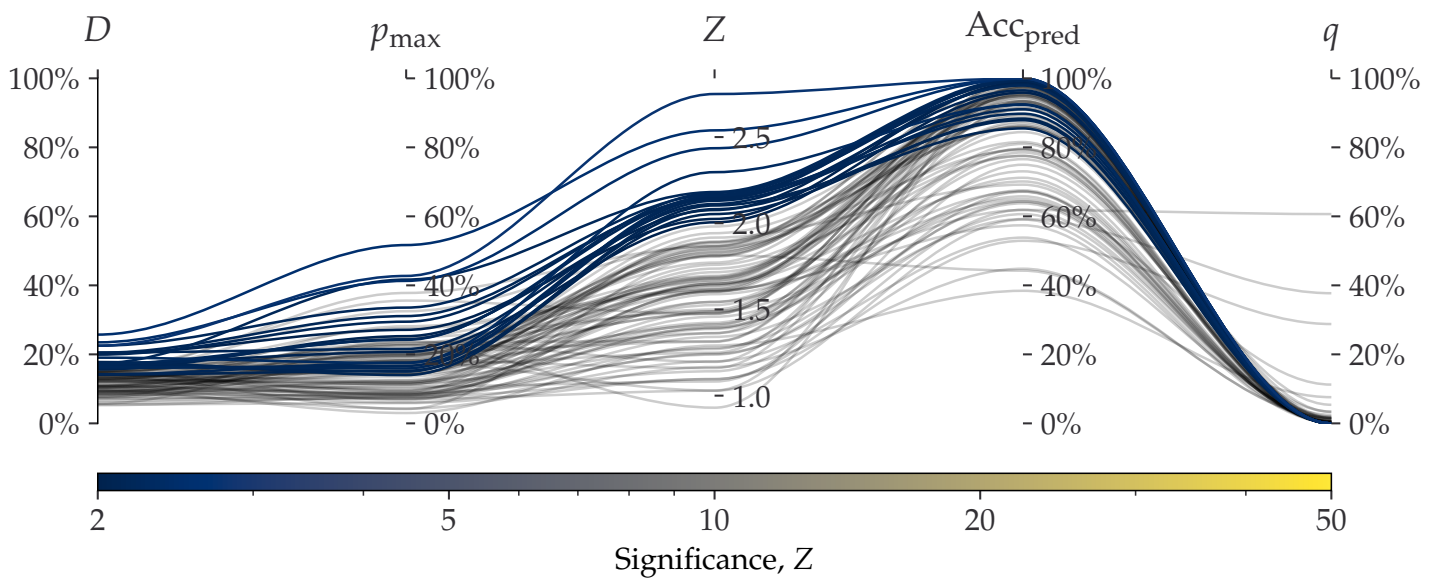


Figure 11. Parallel coordinates plot comparing metaDMG and PyDamage for the Homo Sapiens single-genome simulation with 100 reads and 15% added artificial damage. The two first axes show the estimated damage: D_{fit} by metaDMG and p_{\max} by PyDamage. The following two axes show the fit quality: significance (Z_{fit}) by metaDMG and the predicted accuracy (Acc_{pred}) by PyDamage. The final axis shows the q -value by PyDamage. Each of the 100 replications are plotted as single lines. Replications passing the relaxed metaDMG damage threshold ($D_{\text{fit}} > 1\%$ and $Z_{\text{fit}} > 2$) are shown in color proportional to their significance. Replications that did not pass are shown in semi-transparent black lines.

Table 3. Computational performance of PyDamage and metaDMG. The table contains the times it takes to run either PyDamage or metaDMG on the full Pitch-6 sample containing 11.433 taxa. The timings are shown for both single-processing case (1 core) and multi-processing (2 and 4 cores). The timings were performed on a Macbook M1 Pro model from 2021. “12.6x” means that metaDMG was 12.6 times faster than PyDamage for that particular test.

Cores	Pydamage (s)	metaDMG (s)	Improvement (x)
1	1105	88 s	12.6
2	592	66 s	9.0
4	398	54 s	7.4

researchers to explore their data.

450 Multiple areas of future improvements exists. Currently, our novel test statistic for the damage
451 estimation D_{fit} is based on a statistical model where we only consider the C→T and G→A transitions
452 and where each taxa is modelled as being fully independent, even for closely related species when
453 provided a taxonomic tree. This could be improved upon with the use of a hierarchical model
454 were information across taxonomic leaf nodes is shared. The current implementation, however,
455 allows for easy parallelization of the individual fits which reduces the time spent on the inference.
456 In addition to the mismatch matrices, another improvement would be to include the read length
457 distribution as a covariate in the damage model, as, in addition to deamination, the fragment length
458 distribution is also an indicator of ancient damage (Dabney, Meyer, and Pääbo, 2013; Peyrégne and
459 Prüfer, 2020).

460 We show that the D_{fit} statistic that metaDMG provides is accurate across different damage levels
461 and different number of reads. In the single-genome reference case, we further show that the
462 estimates are stable across different species and fragment length distributions. In addition to this,
463 we find that the results are independent of the contig size, in contrast to PyDamage (Borry et al.,
464 2021).

465 The basis for the D_{fit} statistic is the leaf node mismatch matrices which contains the raw ob-
466 served substitution frequencies. The computation of these could also take into account the com-
467 puted mapping uncertainty and the uncertainty of the assigned called nucleotide. We include a
468 regression approach for stabilizing the mismatch matrices across all covariates but this requires
469 much more data than our current approach. Rather than regressing on all covariates, it might also
470 be more biological meaningfull to regress on the four Briggs parameters.

471 In our toolkit we have included the PMDtools approach (Skoglund et al., 2014) that allows for
472 the separation of highly damaged reads from undamaged reads. The method offers a reasonable
473 way to distinguish the endogenous ancient DNA from possible modern contamination. But this
474 method may suffer from the fact that some fixed empirical parameters are applied. A possible
475 extension can be using several statistics estimated from the specific sample (e.g., taxa specific D_{fit} ,
476 and the ancient fragment lengths) as priors in an empirical Bayes inference framework to learn the
477 categories of reads unsupervisedly.

478 Our research indicate that the metaDMG results are conservative with very low false positive rates.
479 This is particularly important with metagenomic samples as the number of taxa, and thus the num-

480 ber of damage estimates, tend to be large. As the number of fits increases, we strongly believe that
482 a graphical user interface is important. This helps to select and filter the fit results, and to better un-
484 derstand the data at hand. We have tested `metaDMG` using a state of the art metagenomic simulation
pipeline based on multiple metagenomic real-life sample from a variety of different environments.
486 We hope that `metaDMG` can improve the knowledge about DNA damage degradation in different
environments and be the foundation of a more general, metagenomic ancient damage study.

486 6 | AUTHOR CONTRIBUTIONS

CM developed and implemented the damage model and all aspect of the python code including
488 the CLI, all fits, and the dashboard. TP helped develop the model and with statistical discussions.
TSK implemented the C/C++ code relating to the lowest common ancestor and mismatch matrices.
490 LZ implemented the PMDtools and full multinomial regression subfunctionality. AFG and MWP
designed the metagenomic simulation study and the application of `metaDMG` to real data. CM and
492 MWP ran all analyses. CM, MWP and TSK initiated and designed the project. All authors contributed
to writing the manuscript.

494 REFERENCES

- Ardelean, Ciprian F. et al. (2020). "Evidence of human occupation in Mexico around the Last Glacial Maximum". en. In: *Nature* 584.7819. Number: 7819 Publisher: Nature Publishing Group, pp. 87-92. ISSN: 1476-4687. DOI: [10.1038/s41586-020-2509-0](https://doi.org/10.1038/s41586-020-2509-0).
- Betancourt, Michael (2018). "A Conceptual Introduction to Hamiltonian Monte Carlo". In: *arXiv:1701.02434 [stat]*. arXiv: 1701.02434.
- Borry, Maxime et al. (2021). "PyDamage: automated ancient damage identification and estimation for contigs in ancient DNA de novo assembly". en. In: *PeerJ* 9. Publisher: PeerJ Inc., e11845. ISSN: 2167-8359. DOI: [10.7717/peerj.11845](https://doi.org/10.7717/peerj.11845).
- Braadbaart, F. et al. (2020). "Heating histories and taphonomy of ancient fireplaces: A multi-proxy case study from the Upper Palaeolithic sequence of Abri Pataud (Les Eyzies-de-Tayac, France)". en. In: *Journal of Archaeological Science: Reports* 33, p. 102468. ISSN: 2352-409X. DOI: [10.1016/j.jasrep.2020.102468](https://doi.org/10.1016/j.jasrep.2020.102468).
- Bradbury, James et al. (2018). *JAX: composable transformations of Python NumPy programs*.
- Briggs, Adrian W. et al. (2007). "Patterns of damage in genomic DNA sequences from a Neandertal". en. In: *Proceedings of the National Academy of Sciences* 104.37. Publisher: National Academy of Sciences Section: Biological Sciences, pp. 14616–14621. ISSN: 0027-8424, 1091-6490. DOI: [10.1073/pnas.0704665104](https://doi.org/10.1073/pnas.0704665104).
- Cabanski, Christopher R. et al. (2012). "ReQON: a Bioconductor package for recalibrating quality scores from next-generation sequencing data". In: *BMC Bioinformatics* 13.1, p. 221. ISSN: 1471-2105. DOI: [10.1186/1471-2105-13-221](https://doi.org/10.1186/1471-2105-13-221).
- Cepeda-Cuervo, Edilberto and MARÍA VICTORIA Cifuentes-Amado (2017). "Double Generalized Beta-Binomial and Negative Binomial Regression Models". en. In: *Revista Colombiana de Estadística* 40.1. Publisher: Universidad Nacional de Colombia., pp. 141–163. ISSN: 0120-1751. DOI: [10.15444/rce.v40n1.61779](https://doi.org/10.15444/rce.v40n1.61779).
- Dabney, Jesse, Matthias Meyer, and Svante Pääbo (2013). "Ancient DNA Damage". In: *Cold Spring Harbor Perspectives in Biology* 5.7, a012567. ISSN: 1943-0264. DOI: [10.1101/cshperspect.a012567](https://doi.org/10.1101/cshperspect.a012567).
- Dembinski, Hans et al. (2021). *scikit-hep/iminuit: v2.8.2*. DOI: [10.5281/ZENODO.3949207](https://doi.org/10.5281/ZENODO.3949207).

- 522 Fellows Yates, James A. et al. (2021). "The evolution and changing ecology of the African hominid
oral microbiome". en. In: *Proceedings of the National Academy of Sciences* 118.20, e2021655118.
524 ISSN: 0027-8424, 1091-6490. DOI: [10.1073/pnas.2021655118](https://doi.org/10.1073/pnas.2021655118).
- Fernandez-Guerra, Antonio (2022a). *BAM-filter*. original-date: 2021-10-19T09:14:18Z.
- 526 — (2022b). *genomewalker/aMGSIM-smk: v0.0.1*. DOI: [10.5281/zenodo.7298422](https://doi.org/10.5281/zenodo.7298422).
- Ginolhac, Aurelien et al. (2011). "mapDamage: testing for damage patterns in ancient DNA se-
528 quences". In: *Bioinformatics* 27.15, pp. 2153–2155. ISSN: 1367-4803. DOI: [10.1093/bioinformatics/btr347](https://doi.org/10.1093/bioinformatics/btr347).
- 530 Henriksen, Ramus, Lei Zhao, and Thorfinn Korneliussen (2022). *NGSNGS: v0.5.0*. DOI: [10.5281/zenodo.7326212](https://doi.org/10.5281/zenodo.7326212).
- 532 Huang, Weichun et al. (2012). "ART: a next-generation sequencing read simulator". eng. In: *Bioinfor-
matics (Oxford, England)* 28.4, pp. 593–594. ISSN: 1367-4811. DOI: [10.1093/bioinformatics/btr708](https://doi.org/10.1093/bioinformatics/btr708).
- 534 Jensen, Theis Z. T. et al. (2019). "A 5700 year-old human genome and oral microbiome from chewed
birch pitch". en. In: *Nature Communications* 10.1. Number: 1 Publisher: Nature Publishing Group,
536 p. 5520. ISSN: 2041-1723. DOI: [10.1038/s41467-019-13549-9](https://doi.org/10.1038/s41467-019-13549-9).
- Jónsson, Hákon et al. (2013). "mapDamage2.0: fast approximate Bayesian estimates of ancient DNA
538 damage parameters". en. In: *Bioinformatics* 29.13, pp. 1682–1684. ISSN: 1367-4803, 1460-2059.
DOI: [10.1093/bioinformatics/btt193](https://doi.org/10.1093/bioinformatics/btt193).
- 540 Lam, Siu Kwan, Antoine Pitrou, and Stanley Seibert (2015). "Numba: a LLVM-based Python JIT com-
piler". In: *Proceedings of the Second Workshop on the LLVM Compiler Infrastructure in HPC*. LLVM
542 '15. New York, NY, USA: Association for Computing Machinery, pp. 1–6. ISBN: 978-1-4503-4005-2.
DOI: [10.1145/2833157.2833162](https://doi.org/10.1145/2833157.2833162).
- 544 Langmead, Ben and Steven L. Salzberg (2012). "Fast gapped-read alignment with Bowtie 2". en. In:
Nature Methods 9.4. Number: 4 Publisher: Nature Publishing Group, pp. 357–359. ISSN: 1548-
546 7105. DOI: [10.1038/nmeth.1923](https://doi.org/10.1038/nmeth.1923).
- McElreath, Richard (2020). *Statistical rethinking: a Bayesian course with examples in R and Stan*. 2nd ed.
548 CRC texts in statistical science. Boca Raton: Taylor and Francis, CRC Press. ISBN: 978-0-367-
13991-9.
- 550 Mölder, Felix et al. (2021). *Sustainable data analysis with Snakemake*. en. Tech. rep. 10:33. Type: arti-
cle. F1000Research. DOI: [10.12688/f1000research.29032.2](https://doi.org/10.12688/f1000research.29032.2).

- 552 Murchie, Tyler J. et al. (2021). "Collapse of the mammoth-steppe in central Yukon as revealed by
ancient environmental DNA". en. In: *Nature Communications* 12.1. Number: 1 Publisher: Nature
554 Publishing Group, p. 7120. ISSN: 2041-1723. DOI: [10.1038/s41467-021-27439-6](https://doi.org/10.1038/s41467-021-27439-6).
- 556 Nayfach, Stephen et al. (2021). "CheckV assesses the quality and completeness of metagenome-
assembled viral genomes". en. In: *Nature Biotechnology* 39.5. Number: 5 Publisher: Nature Pub-
558 lishing Group, pp. 578–585. ISSN: 1546-1696. DOI: [10.1038/s41587-020-00774-7](https://doi.org/10.1038/s41587-020-00774-7).
- 560 NCBI Resource Coordinators (2018). "Database resources of the National Center for Biotechnology
Information". In: *Nucleic Acids Research* 46.D1, pp. D8–D13. ISSN: 0305-1048. DOI: [10.1093/nar/gkx1095](https://doi.org/10.1093/nar/gkx1095).
- 562 Neukamm, Judith, Alexander Peltzer, and Kay Nieselt (2021). "DamageProfiler: fast damage pattern
calculation for ancient DNA". In: *Bioinformatics* 37.20, pp. 3652–3653. ISSN: 1367-4803. DOI: [10.1093/bioinformatics/btab190](https://doi.org/10.1093/bioinformatics/btab190).
- 564 Parks, Donovan H. et al. (2018). "A standardized bacterial taxonomy based on genome phylogeny
substantially revises the tree of life". en. In: *Nature Biotechnology* 36.10. Number: 10 Publisher:
566 Nature Publishing Group, pp. 996–1004. ISSN: 1546-1696. DOI: [10.1038/nbt.4229](https://doi.org/10.1038/nbt.4229).
- 568 Pedersen, Mikkel et al. (2016). "Postglacial viability and colonization in North America's ice-free
corridor". en. In: *Nature* 537.7618. Number: 7618 Publisher: Nature Publishing Group, pp. 45–
570 49. ISSN: 1476-4687. DOI: [10.1038/nature19085](https://doi.org/10.1038/nature19085).
- 572 Peyrégne, Stéphane and Kay Prüfer (2020). "Present-Day DNA Contamination in Ancient DNA Datasets".
en. In: *BioEssays* 42.9. _eprint: <https://onlinelibrary.wiley.com/doi/pdf/10.1002/bies.202000081>,
p. 2000081. ISSN: 1521-1878. DOI: [10.1002/bies.202000081](https://doi.org/10.1002/bies.202000081).
- 574 Phan, Du, Neeraj Pradhan, and Martin Jankowiak (2019). "Composable Effects for Flexible and Accel-
erated Probabilistic Programming in NumPyro". In: *arXiv:1912.11554 [cs, stat]*. arXiv: 1912.11554.
- 576 Plotly, Technologies (2015). *Collaborative data science*. Place: Montreal, QC Publisher: Plotly Tech-
nologies Inc.
- 578 Renaud, Gabriel et al. (2017). "gargamel: a sequence simulator for ancient DNA". eng. In: *Bioinfor-
matics (Oxford, England)* 33.4, pp. 577–579. ISSN: 1367-4811. DOI: [10.1093/bioinformatics/btw670](https://doi.org/10.1093/bioinformatics/btw670).
- Schulte, Luise et al. (2021). "Hybridization capture of larch (*Larix Mill.*) chloroplast genomes from
580 sedimentary ancient DNA reveals past changes of Siberian forest". en. In: *Molecular Ecology Re-
sources* 21.3. _eprint: <https://onlinelibrary.wiley.com/doi/pdf/10.1111/1755-0998.13311>, pp. 801–
582 815. ISSN: 1755-0998. DOI: [10.1111/1755-0998.13311](https://doi.org/10.1111/1755-0998.13311).

- Skoglund, Pontus et al. (2014). "Separating endogenous ancient DNA from modern day contamination in a Siberian Neandertal". In: *Proceedings of the National Academy of Sciences* 111.6. Publisher: Proceedings of the National Academy of Sciences, pp. 2229–2234. DOI: [10.1073/pnas.1318934111](https://doi.org/10.1073/pnas.1318934111).
- Valk, Tom van der et al. (2021). "Million-year-old DNA sheds light on the genomic history of mammoths". en. In: *Nature* 591.7849. Number: 7849 Publisher: Nature Publishing Group, pp. 265–269. ISSN: 1476-4687. DOI: [10.1038/s41586-021-03224-9](https://doi.org/10.1038/s41586-021-03224-9).
- Vernot, Benjamin et al. (2021). "Unearthing Neanderthal population history using nuclear and mitochondrial DNA from cave sediments". In: *Science* 372.6542. Publisher: American Association for the Advancement of Science, eabf1667. DOI: [10.1126/science.abf1667](https://doi.org/10.1126/science.abf1667).
- Wang, Yucheng, Thorfinn Sand Korneliussen, et al. (2022). "ngsLCA—A toolkit for fast and flexible lowest common ancestor inference and taxonomic profiling of metagenomic data". In: *Methods in Ecology and Evolution* n/a.n/a. Publisher: John Wiley & Sons, Ltd. ISSN: 2041-210X. DOI: [10.1111/2041-210X.14006](https://doi.org/10.1111/2041-210X.14006).
- Wang, Yucheng, Mikkel Pedersen, et al. (2021). "Late Quaternary dynamics of Arctic biota from ancient environmental genomics". en. In: *Nature* 600.7887. Number: 7887 Publisher: Nature Publishing Group, pp. 86–92. ISSN: 1476-4687. DOI: [10.1038/s41586-021-04016-x](https://doi.org/10.1038/s41586-021-04016-x).
- Zavala, Elena I. et al. (2021). "Pleistocene sediment DNA reveals hominin and faunal turnovers at Denisova Cave". en. In: *Nature* 595.7867. Number: 7867 Publisher: Nature Publishing Group, pp. 399–403. ISSN: 1476-4687. DOI: [10.1038/s41586-021-03675-0](https://doi.org/10.1038/s41586-021-03675-0).

Appendix 1

PMDTOOLS

Three non-mutually exclusive events can lead to an observation of C→T or G→A (Skoglund et al., 2014), namely (i) a true biological polymorphism (occurring at rate π), (ii) a sequencing errors (rate ϵ , can be extracted from the base quality scores of the site on the sampled strand), and (iii) in the case of damaged DNA, the damaged nucleotide frequencies are assumed to be only related to its position from either termini of the ancient fragment (C→T from 5' end, and G→A from 3' end). The error probability of the postmortem nucleotide misincorporation is under the pmdtools model given by:

$$D_x = C + p(1 - p)^{|x|}, \quad (10)$$

here $C = 0.01$ and $p = 0.3$ are both suitable constants. Skoglund et al., 2014 defines the likelihood ratio of a strand between the PMD model and the NULL model as its postmortem damage score (PMDS),

$$\text{PMDS} = \log \left\{ \frac{\prod_x L(\text{PMD} | S_x)}{\prod_x L(\text{NULL} | S_x)} \right\}, \quad (11)$$

The reads with the PMDS exceeding an empirical p-value threshold can then be used for filtering intensively damaged fragments.

Appendix 2

MULTINOMIAL LOGISTIC REGRESSIONS

Full Multinomial Logistic Regression

Postmortem damages have impacts on the next generation sequencing reads. A common phenomenon is the increasing of the calling error rates from nucleotide C→T due to the cytosine deamination process. Unawareness of this will lead to inaccurate inferences. Evidences show that the magnitude of such changes are related to the positions the site is within a read (the fraction of the ancient DNA). Here we present four slightly different ways (i.e., full unconditional regression, full conditional regression, folded unconditional regression and folded conditional regression) to unveil the relationship between the calling error rates and the mismatching reference/read pairs as well as the site positions within a read. The methods are based on the multinomial logistic regressions.

Data Description

We perform the regressions based on the summary statistic of the mismatch matrix,i.e., $M(x)$, which is a table which contains the counts of reads of different reference/read categories (in total 16) and positions on the forward/reversed strand (15 positions on each direction). *Table S1* and *Table S2* give an example of the data format we use for the inference.

Ref.	Read Counts							
	A				C			
Read	A	C	G	T	A	C	G	T
1	12794053	8325	28769	16073	10404	8045811	8020	2092619
2	13480290	6812	21107	12102	9151	8260185	6531	1145605
3	12760253	6131	18859	10327	7772	8385423	5899	914709
4	12995572	5240	17671	8940	7880	8345892	5252	767237
5	12930102	4601	17021	8188	8374	8474964	5161	703283
6	12879355	4684	16435	7536	8726	8571141	4811	643607
7	12684349	4557	15298	7394	8835	8727254	4762	586674
8	12585563	4454	15497	7236	8898	8888173	5058	527691
9	12468622	4309	14704	6942	8948	9076851	4673	481170
10	12491183	4437	14567	6912	9103	9237982	4702	443329
11	12430899	4296	14083	6515	9313	9364121	4609	404431
12	12419506	4226	13985	6503	9342	9357468	4367	371475
13	12469412	4147	13851	6375	9586	9386737	4588	345390
14	12549936	4045	13650	6246	9673	9324488	4628	322294
15	12566555	4174	13499	6213	9735	9305820	4518	301360
-1	11599167	8800	16164	14851	90888	9613102	10843	19810
-2	11985637	8769	14044	12040	28799	9561124	7184	18424
-3	12941743	7805	13861	12001	24988	9400151	6368	15466
-4	12808985	7141	12885	9889	23067	9509723	5421	14901
-5	12869585	6954	12100	9428	22349	9464831	5789	13987
-6	12784911	6440	12080	8735	20556	9566794	6544	14021
-7	12878349	5946	12311	8225	19480	9566359	6478	16419
-8	12719722	9521	12156	8131	19226	9725468	6709	23434
-9	12652860	5634	11940	7671	18035	9762224	6321	31667
-10	12566817	5448	11850	7178	17353	9701382	6306	37831
-11	12702498	5309	12092	7568	16121	9526031	6035	43215
-12	12731940	5207	11933	6856	15637	9533858	5557	47650
-13	12697647	4989	12199	7153	15072	9508117	5434	51614
-14	12689924	4944	11891	6816	15050	9525285	5237	55598
-15	12660634	4746	11753	6732	14815	9561359	5184	59633

642

Appendix 2—table S1. The read counts per position given the reference nucleotides are A or C of an ancient human data. The negative position indices are the position on the reversed strand. In the manuscript, the elements (the values of a specific nucleotide read counts per position given the reference nucleotide is A or C) in this table are denoted as $M_{A-i}(x)$ or $M_{C-i}(x)$.

644

646

Ref.	Read Counts							
	G				T			
Read	A	C	G	T	A	C	G	T
1	16389	8976	9639767	86584	11733	15878	8351	11718463
2	17614	6483	9510149	26655	10761	13958	7011	11974947
3	15164	5949	9488917	23374	9509	13767	6046	12839015
4	14844	5186	9566468	21960	8170	12509	5585	12721790
5	14005	5612	9497118	20468	7186	11991	5233	12795244
6	13671	6195	9622572	19096	6948	11683	4790	12686645
7	16648	6394	9609855	18594	6203	12122	4780	12794172
8	23659	6405	9768666	17341	6131	11847	4758	12626614
9	31680	6139	9785449	17034	5998	12040	4469	12579260
10	38484	5982	9700857	16235	5487	11546	4175	12513653
11	44665	5722	9536341	15284	5651	12044	4176	12646627
12	48949	5371	9547134	14569	5449	11663	4060	12684645
13	53076	5234	9543953	14090	5262	11785	4046	12631297
14	57343	5186	9551477	13855	5257	11768	4006	12624840
15	61236	5137	9583481	13667	5122	11733	3947	12612416
-1	2078554	7947	8096447	11847	15732	28461	8551	12890628
-2	1138478	6656	8232666	10760	12299	20759	6999	13446882
-3	921712	5970	8399013	8643	10514	18226	6564	12718084
-4	775038	5720	8319235	8416	9415	17800	5388	12977322
-5	710955	5499	8462058	8926	8526	17088	4911	12886576
-6	647761	5052	8545455	9193	7640	16351	4879	12852322
-7	593854	4872	8693834	9318	7600	15523	5048	12664576
-8	535542	7828	8889921	9399	7163	18704	4718	12510123
-9	486549	4696	9075263	9522	7109	14547	4611	12409220
-10	448895	4622	9226758	9432	6816	14567	4668	12438344
-11	409027	4654	9352528	9544	6575	14019	4611	12388650
-12	376069	4637	9344701	9419	6511	13874	4486	12390148
-13	350609	4655	9384853	9885	6197	13877	4327	12432024
-14	326760	4595	9337266	9889	5986	13928	4403	12490990
-15	305014	4541	9310617	10065	5919	13442	4232	12529684

648 **Appendix 2—table S2.** The read counts per position given the reference nucleotides are G or T of the
 649 same human data as in Table S1. The negative position indices are the position on the reversed
 650 strand. In the manuscript, the elements (the values of a specific nucleotide read counts per position
 651 given the reference nucleotide is G or T) in this table are denoted as $M_{G \rightarrow i}(x)$ or $M_{T \rightarrow i}(x)$.

652

The terminology used here might not be standard. The term full regression here is to distinguish itself from the folded regression discussed later, which simply means inferring the coefficients of forward strand and reversed strand separately. Full regression includes both unconditional regression and conditional regression. The unconditional regression's objective is to infer the probability of observing a read of nucleotide j and its reference is i at position x , i.e., $P_{i \rightarrow j}(x)$ while the conditional regression's target is to estimate the probability of observing a read of nucleotide j given its reference is i at position x , i.e., $P_{j|i}(x)$. Their

relationship is as follows:

$$P_{j|i}(x) = \frac{P_{i \rightarrow j}(x)}{\sum_{j \in \mathcal{B}} P_{i \rightarrow j}(x)}.$$

So in fact, unconditional regression can give us more detailed inferred results (extra information the nucleotide composition per position of the reference, which may be related to the prepared libraries).

670

Unconditional Regression Likelihood

672

The unconditional regression's log-likelihood function is defined as follows,

674

$$\begin{aligned} l_{\text{uncond}} &= \sum_x \sum_{i,j \in \mathcal{B}} M_{i \rightarrow j}(x) \log P_{i \rightarrow j}(x) \\ &= \sum_x \left[M(x) \log P_{T \rightarrow T}(x) + \sum_{(i,j) \neq (T,T)} M_{i \rightarrow j}(x) \log \frac{P_{i \rightarrow j}(x)}{P_{T \rightarrow T}(x)} \right], \end{aligned} \quad (12)$$

676

where $M(x) = \sum_{i,j \in \mathcal{B}} M_{i \rightarrow j}(x)$. According to the multinomial logistic regression, we assume,

$$\log \frac{P_{i \rightarrow j}(x)}{P_{T \rightarrow T}(x)} = \sum_{n=0}^{\text{order}} \alpha_{i,j,x,n} x^n \quad (13)$$

678

Applying Equation 13 to Equation 12, we have

680

$$l_{\text{uncond}} = \sum_x \left\{ -M(x) \log \left[1 + \sum_{(i,j) \neq (T,T)} \exp \left(\sum_{n=0}^{\text{order}} \alpha_{i,j,x,n} x^n \right) \right] + \sum_{(i,j) \neq (T,T)} M_{i \rightarrow j}(x) \sum_{n=0}^{\text{order}} \alpha_{i,j,x,n} x^n \right\} \quad (14)$$

682

The number of inferred parameters ($\alpha_{i,j,x,n}$), for the full conditional regression is $30 \times (\text{order} + 1)$.

684

And the relevant derivatives of the unconditional regression likelihood are as follows,

$$\frac{\partial l_{\text{uncond}}}{\partial \alpha_{i,j,x,n}} = -M(x) \frac{x^n \exp \left(\sum_{n=0}^{\text{order}} \alpha_{i,j,x,n} x^n \right)}{1 + \sum_{(i,j) \neq (T,T)} \exp \left(\sum_{n=0}^{\text{order}} \alpha_{i,j,x,n} x^n \right)} + M_{i \rightarrow j}(x) x^n. \quad (15)$$

Conditional Regression Likelihood

Viewed as the sum of log-likelihoods given the reference nucleotide $i \in \mathcal{B}$, the conditional regression's log-likelihood function is,

$$\begin{aligned} l_{\text{cond}} &= \sum_{i \in \mathcal{B}} \sum_x \sum_{j \in \mathcal{B}} M_{i \rightarrow j}(x) \log P_{j|i}(x) \\ &= \sum_{i \in \mathcal{B}} \sum_x \left[M_i(x) \log P_{T|i}(x) + \sum_{j \neq T} M_{i \rightarrow j}(x) \log \frac{P_{j|i}(x)}{P_{T|i}(x)} \right], \end{aligned} \quad (16)$$

694

where $M_i(x) = \sum_{j \in B} M_{i \rightarrow j}(x)$. Furthermore, if we assume,

$$\log \frac{P_{j|i}(x)}{P_{T|i}(x)} = \sum_{n=0}^{\text{order}} \beta_{i,j,x,n} x^n \quad (17)$$

696

By applying Equation 17 to Equation 16, we can obtain,

698

$$l_{\text{cond}} = \sum_{i \in B} \sum_x \left\{ -M_i(x) \log \left[1 + \sum_{j \neq T} \exp \left(\sum_{n=0}^{\text{order}} \beta_{i,j,x,n} x^n \right) \right] + \sum_{j \neq T} M_{i \rightarrow j}(x) \sum_{n=0}^{\text{order}} \beta_{i,j,x,n} x^n \right\} \quad (18)$$

700

The number of inferred parameters ($\beta_{i,j,x,n}$) for the full unconditional regression is $24 \times (\text{order} + 1)$. And the relevant derivatives of the conditional likelihood are as follows,

702

$$\frac{\partial l_{\text{cond}}}{\partial \beta_{i,j,x,n}} = -M_i(x) \frac{x^n \exp \left(\sum_{n=0}^{\text{order}} \beta_{i,j,x,n} x^n \right)}{1 + \sum_{j \neq T} \exp \left(\sum_{n=0}^{\text{order}} \beta_{i,j,x,n} x^n \right)} + M_{i \rightarrow j}(x) x^n. \quad (19)$$

704

Folded Multinomial Logistic Regression

706

The folded regressions use the same log-likelihood functions as the full regression (i.e., Equation 14 and 18) but are conducted based on a presumable symmetric PMD pattern, i.e., the probability of $C \rightarrow T$ at the position x of an random chosen ancient DNA strand is assumed to equal to the probability of $G \rightarrow A$ at the position $-x$. Such an theoretical assumption go match the current ancient library preparation process (Dabney, Meyer, and Pääbo, 2013; Henriksen, Zhao, and T. Korneliussen, 2022).

708

710

$$\alpha_{i,j,x,n} = \alpha_{c(i),c(j),-x,n}, \quad (20)$$

712

$$\beta_{i,j,x,n} = \beta_{c(i),c(j),-x,n}, \quad (21)$$

714

where $c(i)$ means the complimentary nucleotide of the nucleotide i , e.g., $c(A) = T$ and $c(G) = C$.

716

718

By doing the folded regression, we halve the number of inferred parameters ($\alpha_{i,j,x,n}$ or $\beta_{i,j,x,n}$). Hence The number of inferred parameters for the folded unconditional regression is $15 \times (\text{order} + 1)$, and that of folded conditional regression is $12 \times (\text{order} + 1)$.

Results for multinomial logistic regression

The optimization of the likelihood functions are based on the C++ library of gsl and use the function `gsl_multimin_fminimizer_nmsimplex2` with the initial searching point set to be the results of logistic regression. We here present here 4 figures pertaining to showcase the

724 performance of our model. The regression methods are based on the summary statistic

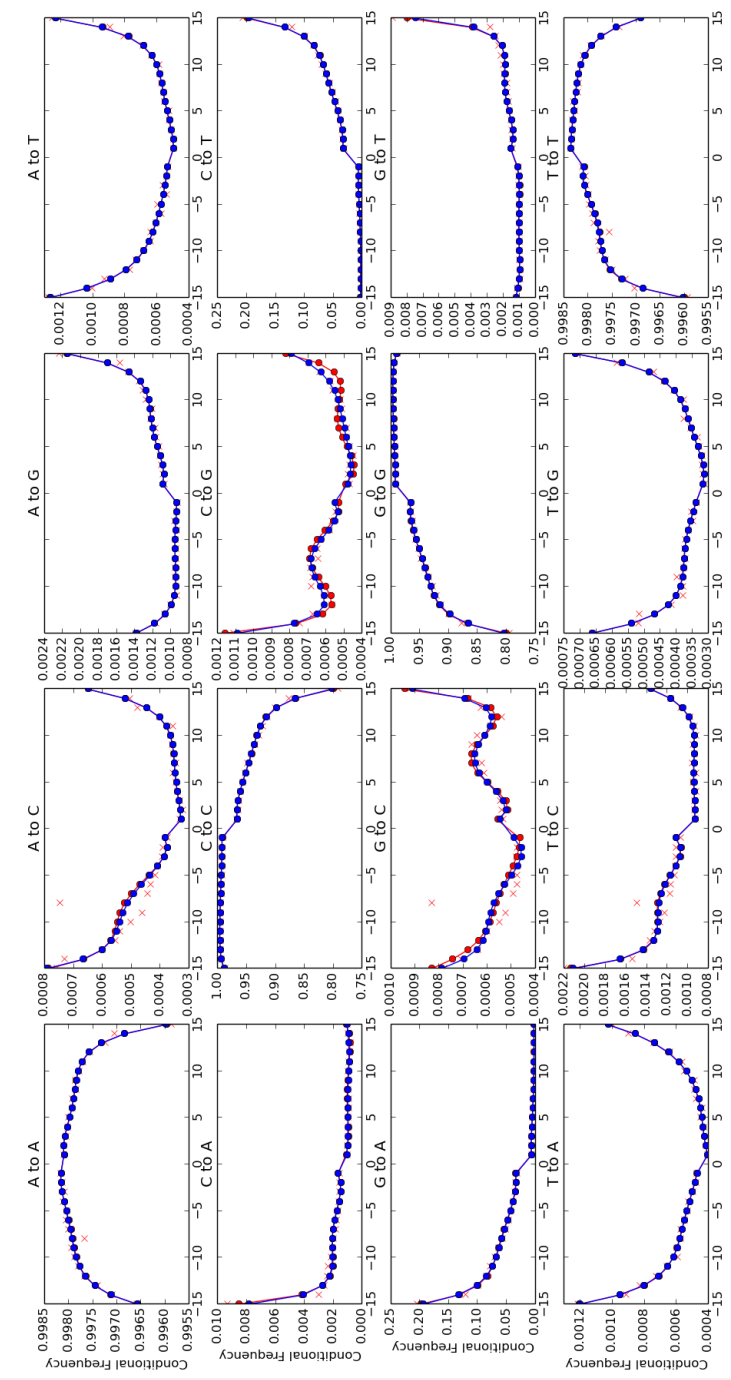
of the counts of mismatches and the optimization is therefore in the scale of milliseconds.

726 *Figure S1* and *Figure S2* are the conditional regression results of the ancient and control

human data correspondingly. And *Figure S3* and *Figure S4* are the folded conditional re-

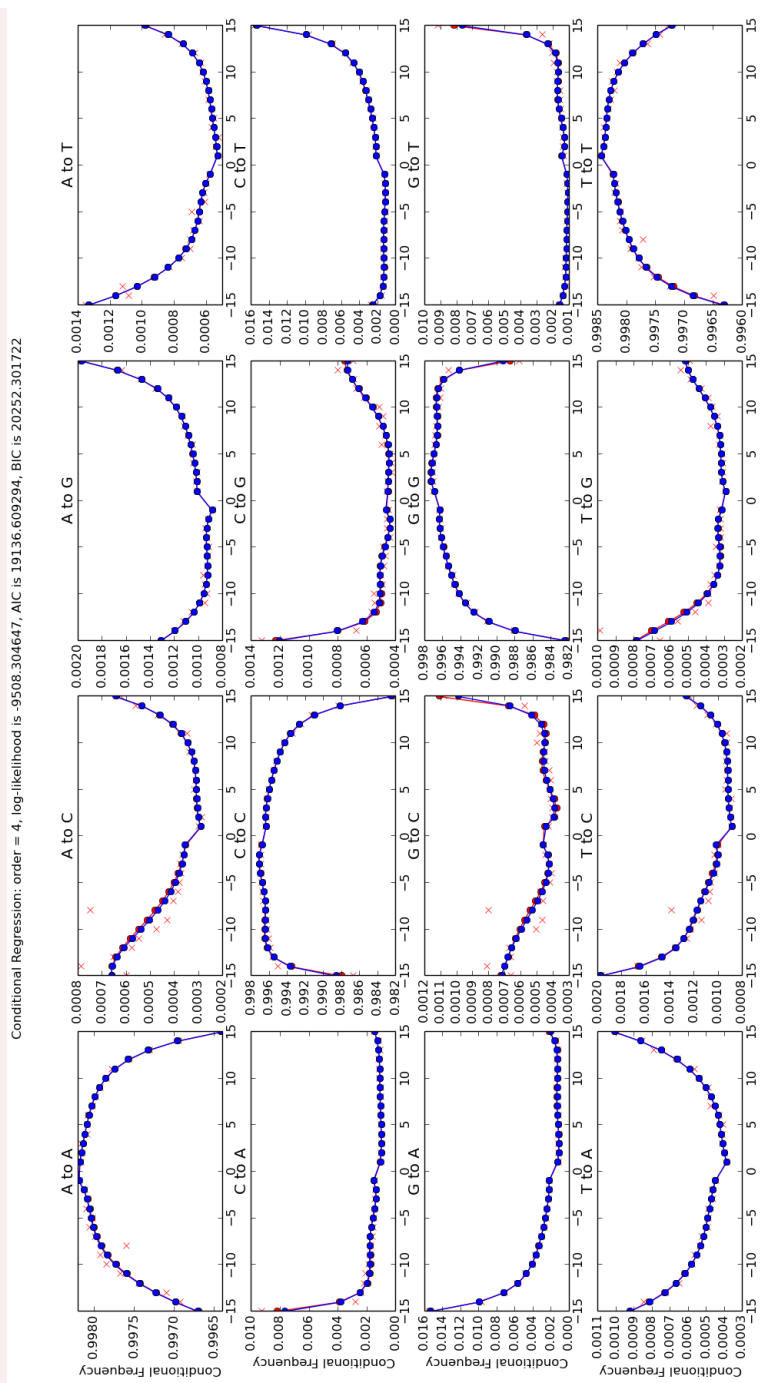
gression results of the same data as above.

Conditional Regression: order = 4, log-likelihood is -34526.568889, AIC is 69173.137778, BIC is 70313.881805



Appendix 2—figure S1. Conditional regression results with the order 4 of the ancient human data.

Each panel of figure represents a specific reference/read pair and plots its frequency across different positions. The positions from left to right are -1 to -15 and 15 to 1 .

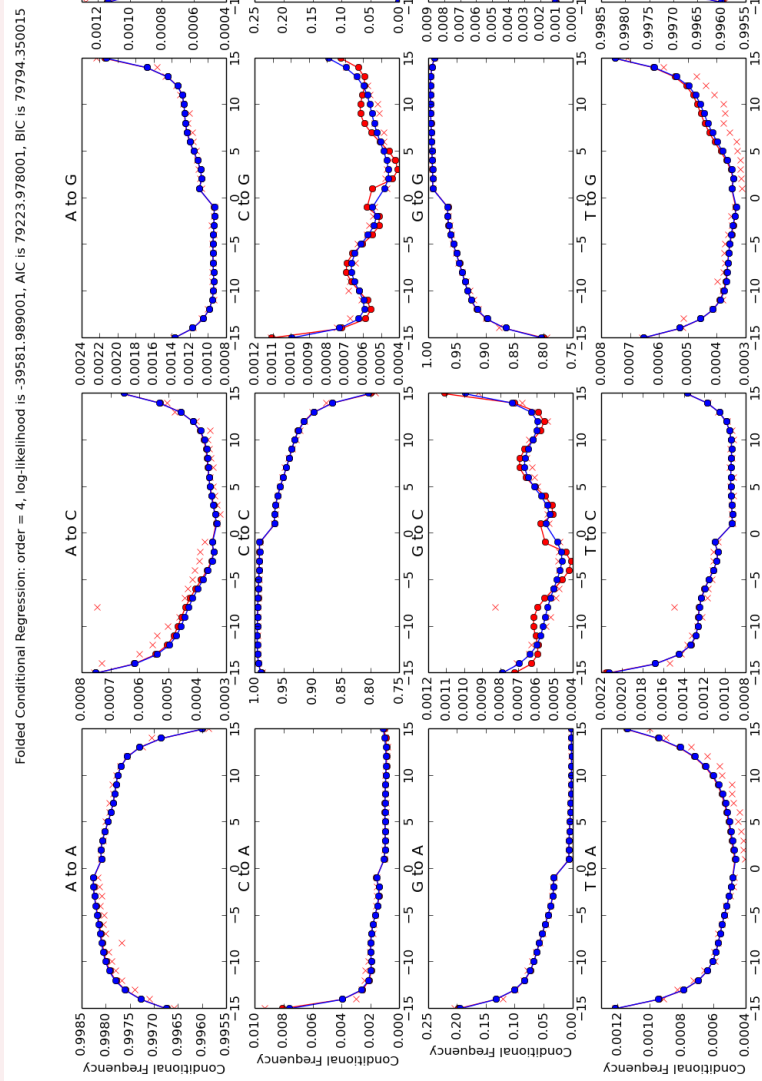


734

Appendix 2—figure S2. Conditional regression results with the order 4 of the control human data.

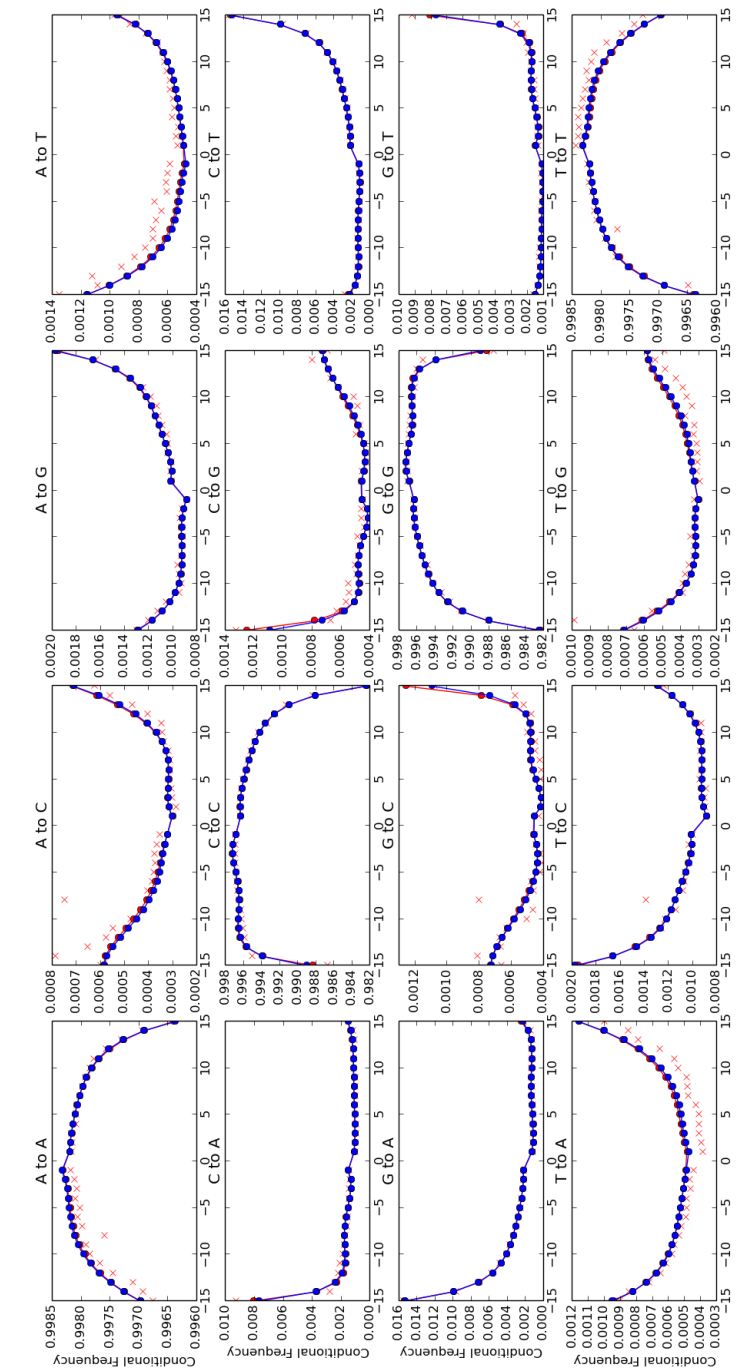
Each panel of figure represents a specific reference/read pair and plots its frequency across different positions. The positions from left to right are -1 to -15 and 1 to 15 .

736



Appendix 2—figure S3. Folded conditional regression results with the order 4 of the ancient human data. Each panel of figure represents a specific reference/read pair and plots its frequency across different positions. The positions from left to right are -1 to -15 and 15 to 1 .

Folded Conditional Regression: order = 4, log-likelihood is -14870.765524, AIC is 29801.531048, BIC is 30359.377262



744

Appendix 2—figure S4. Folded conditional regression results with the order 4 of the control human data. Each panel of figure represents a specific reference/read pair and plots its frequency across different positions. The positions from left to right are -1 to -15 and 15 to 1 .

746

748 As shown in the figures, the regression models stabilize the coarse mismatch matrices
750 and describe a much more detailed PMD pattern (not only C→T and G→A, but also all other
752 reference and read combinations), but they might suffer from an overfitting issue espe-
754 cially when the data is limited, while the simpler regression model in the main text (*sub-*
section 2.4) shows an acceptable statistic power even with extremely small amount of data,
we thus recommend the readers to use the simpler regression model unless used with ex-
tremely high-coverage data.

756 Our code can also perform the unconditional regression, but as the unconditional regres-
sion needs to estimate more parameters based on the same dataset, it is more vulnerable
to a possible overfitting issue. We thus only present the figures of the conditional results.

NGSNGS COMMANDS

760 The resulting read data files (fastq files) were simulated with NGSNGS using the above
761 mentioned simulation parameters, all with the same quality scores profiles as used in ART
762 (Huang et al., 2012), based on the Illumina HiSeq 2500 (150 bp). The mapping was performed
using Bowtie-2 (Langmead and Salzberg, 2012):

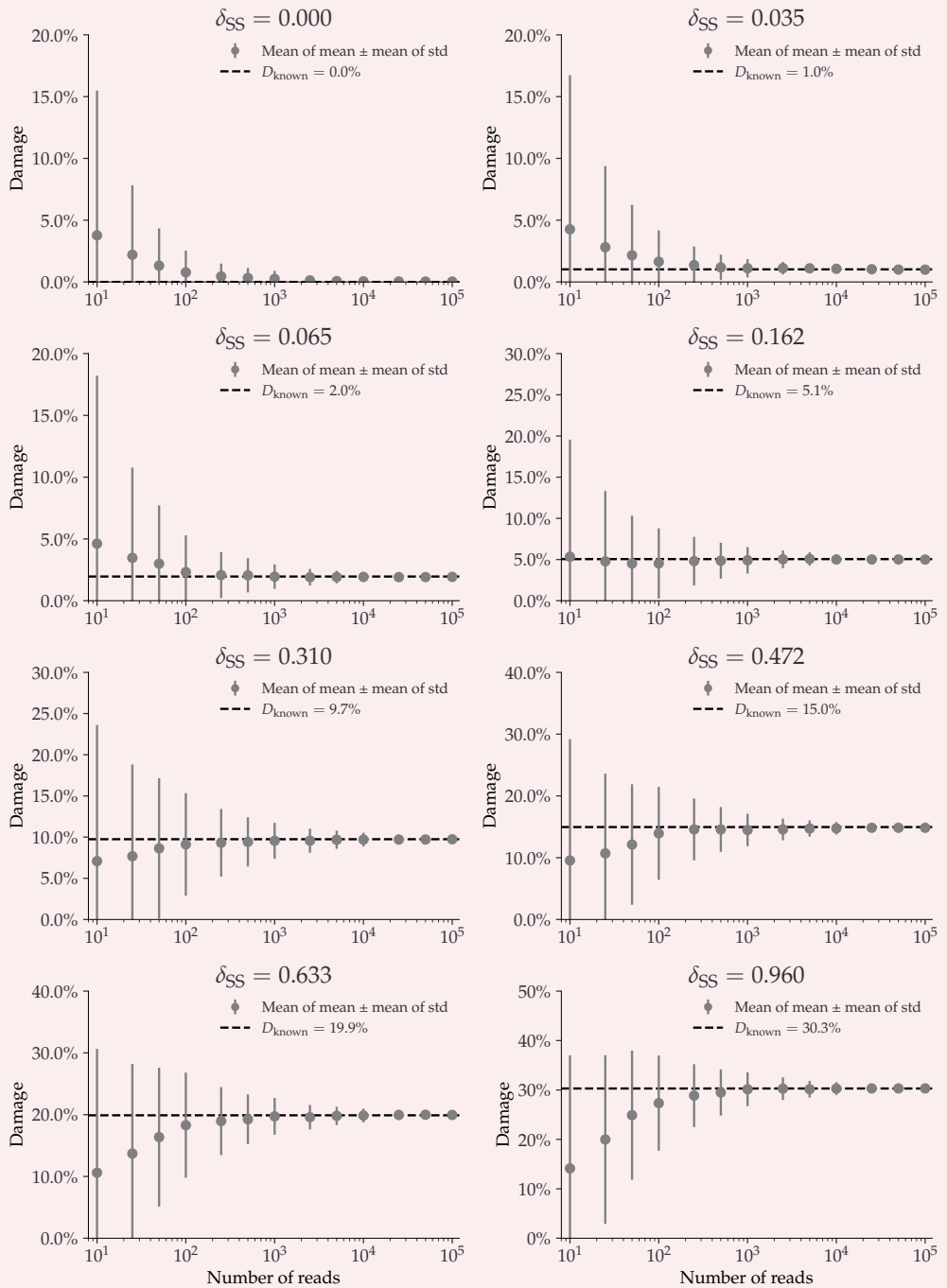
```
764 ./ngsngs -i $genome -r $Nread -ld LogNorm,$lognorm_mean,$lognorm_std -seq SE \  
765 -f fq -q1 $quality_scores -m b,0.024,0.36,$damage,0.0097 -o $fastq  
766 bowtie2 -x $genome -q $fastq.fq --no-unal
```

Appendix 4

768 NGSNGS SIMULATIONS

770 The following figures show the metaDMG damage estimates for the different NGSNGS simu-
772 lations (Henriksen, Zhao, and T. Korneliussen, 2022). These simulations include different
species (*Homo Sapiens* and *Betula*), different GC-levels (low, middle, high), different frag-
ment length distributions (with mean 35, 60, and 90), and different contig lengths (length
1.000, 10.000, 100.000), see **subsection 3.1** for more information.

Homo



774

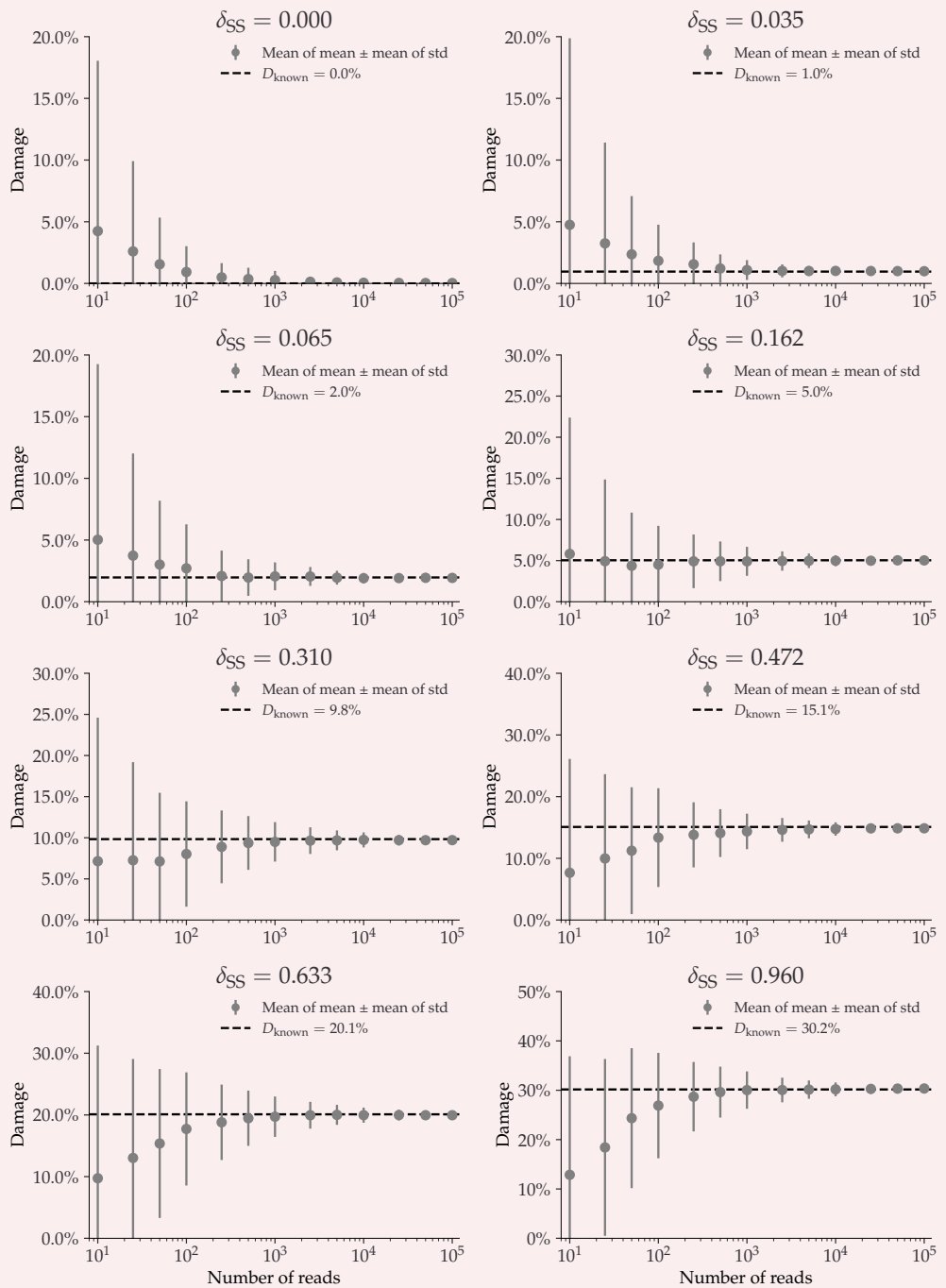
Appendix 4—figure S5. This plot shows the average damage as a function of the number of reads.

776

The grey points show the average of the individual means (with the average of the standard deviations as errors).

778

Betula

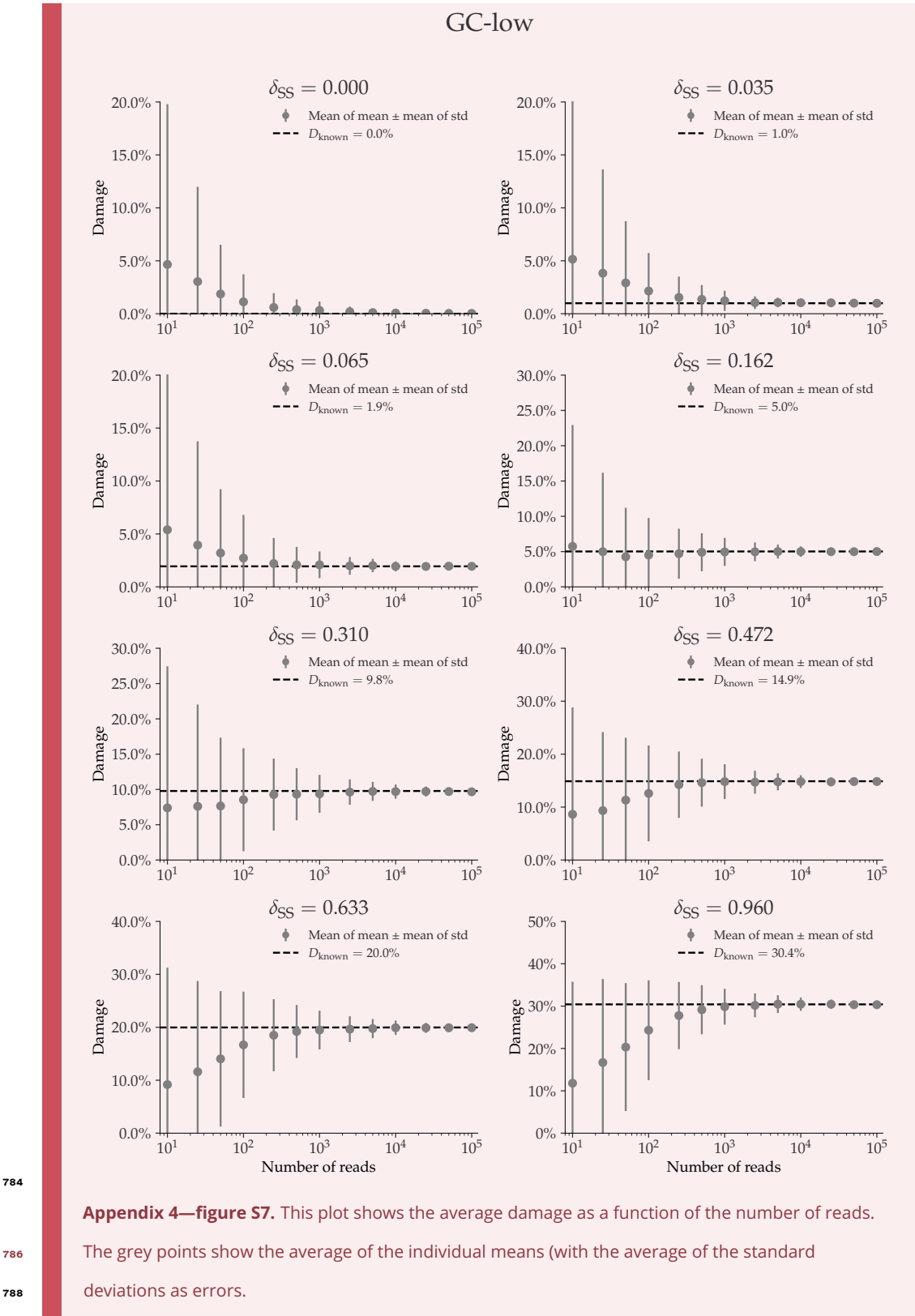


780

Appendix 4—figure S6. This plot shows the average damage as a function of the number of reads.

782

The grey points show the average of the individual means (with the average of the standard deviations as errors).

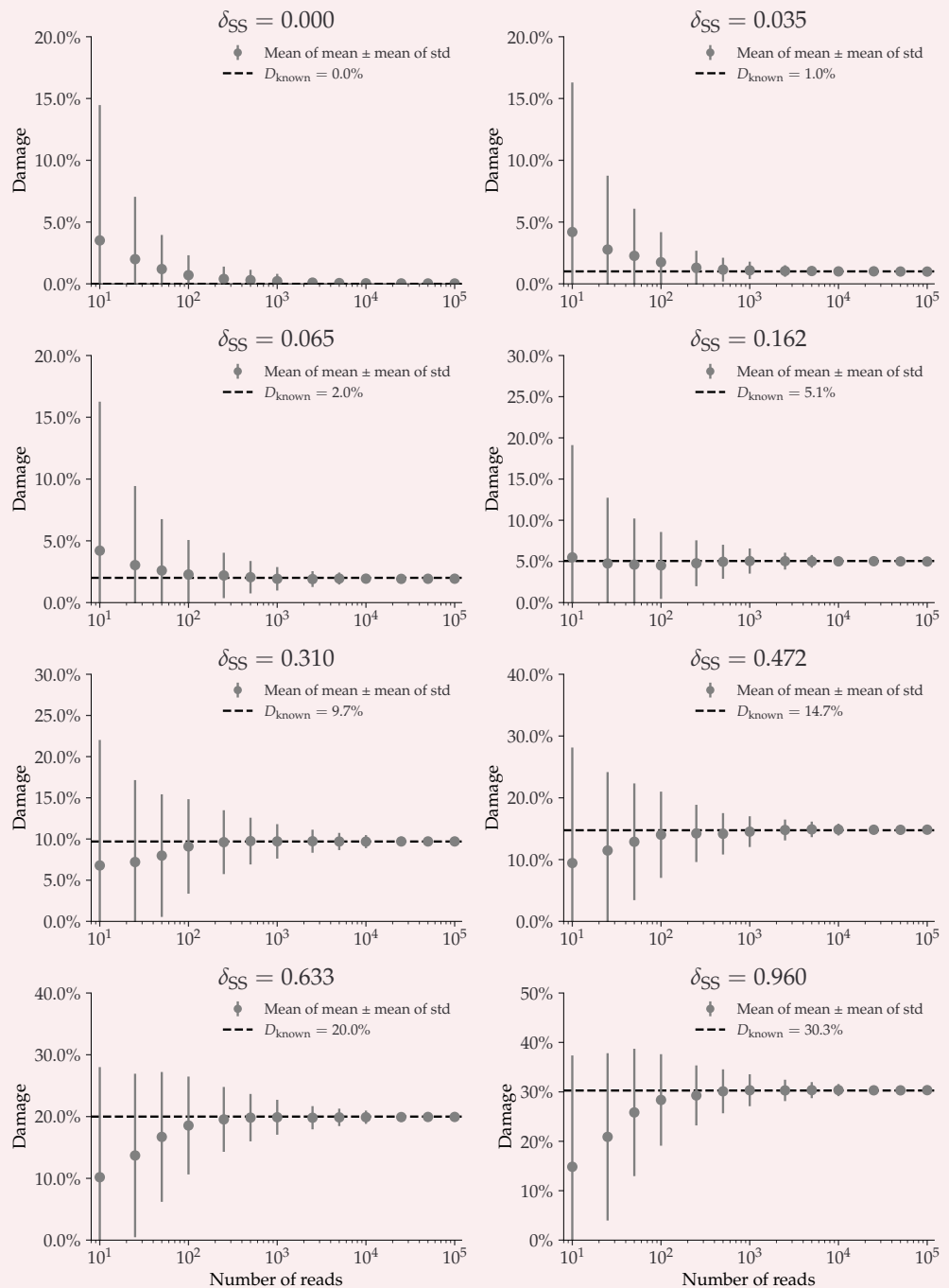


784

786

788

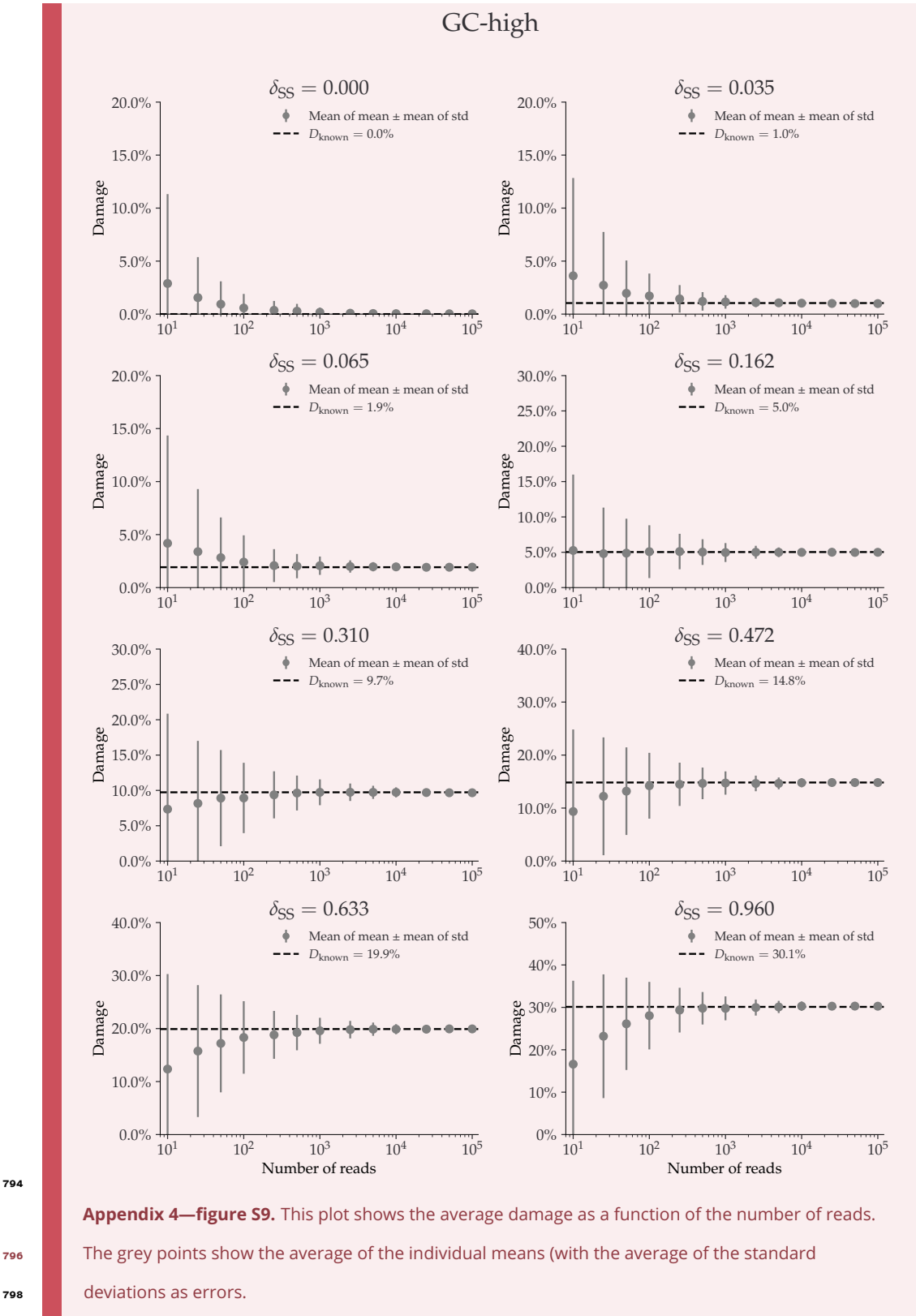
GC-mid



790

Appendix 4—figure S8. This plot shows the average damage as a function of the number of reads. The grey points show the average of the individual means (with the average of the standard deviations as errors).

792

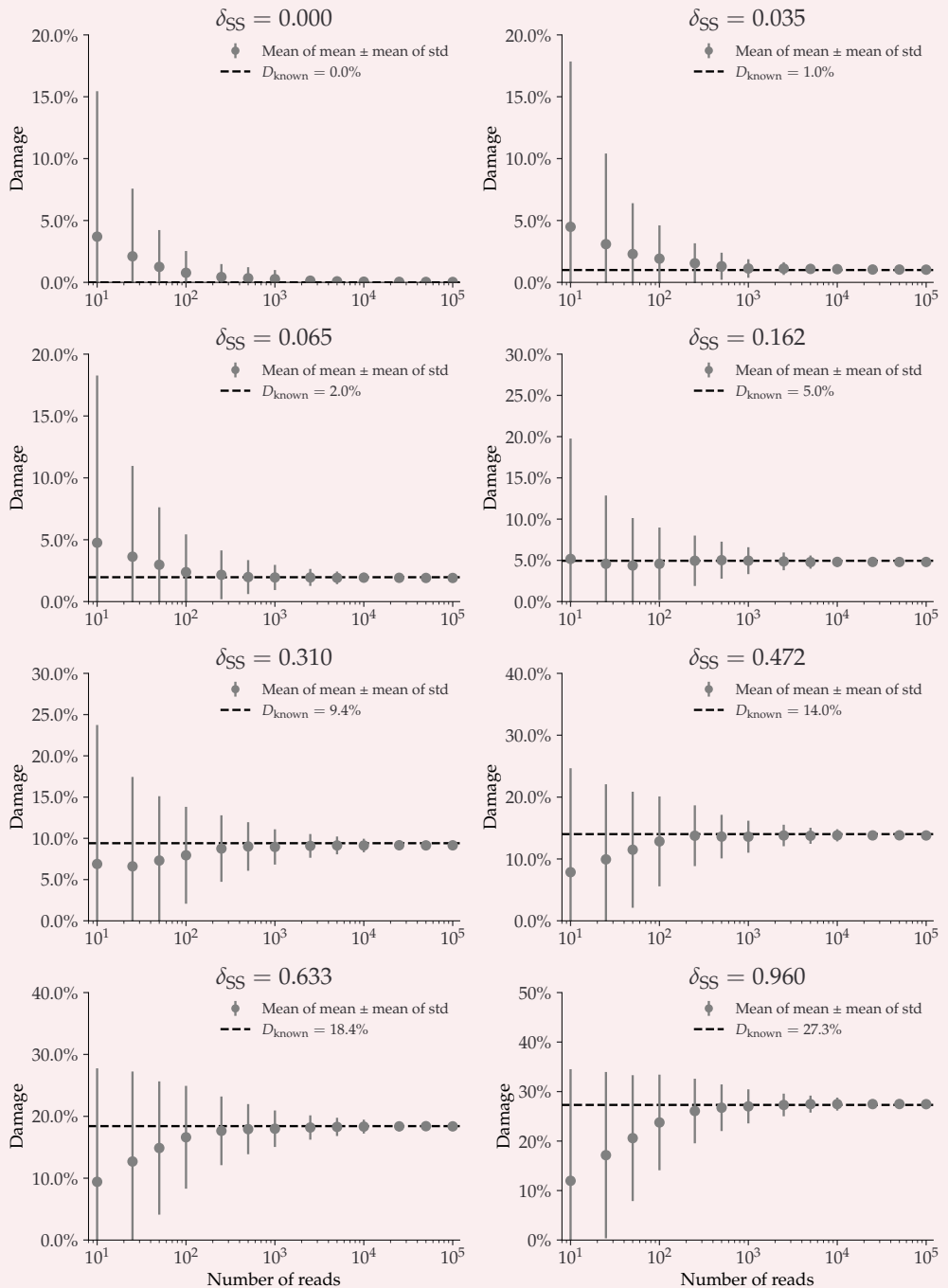


794

796

798

Fragment Length Average: 35



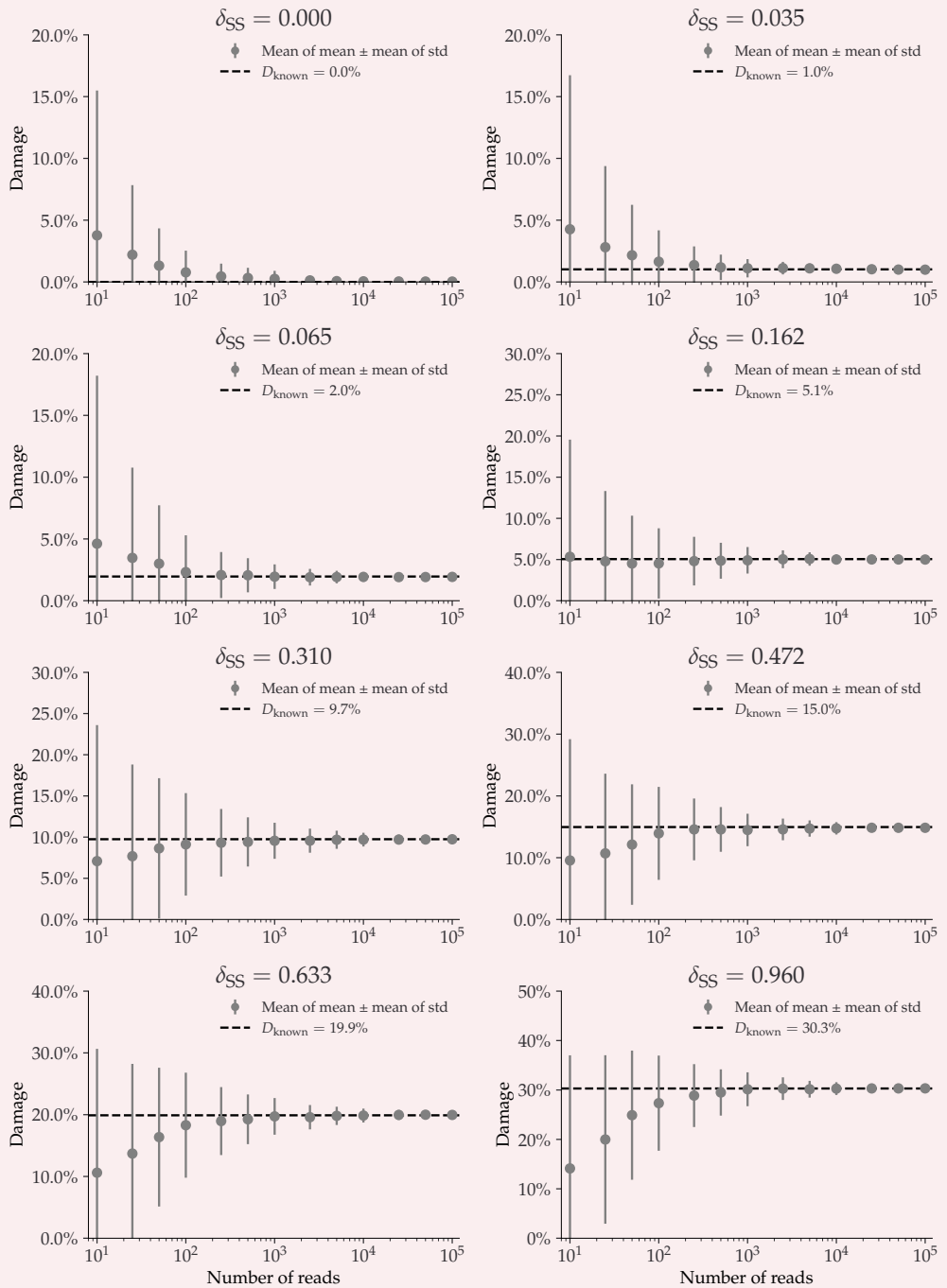
800

Appendix 4—figure S10. This plot shows the average damage as a function of the number of reads.

802

The grey points show the average of the individual means (with the average of the standard deviations as errors).

Fragment Length Average: 60



804

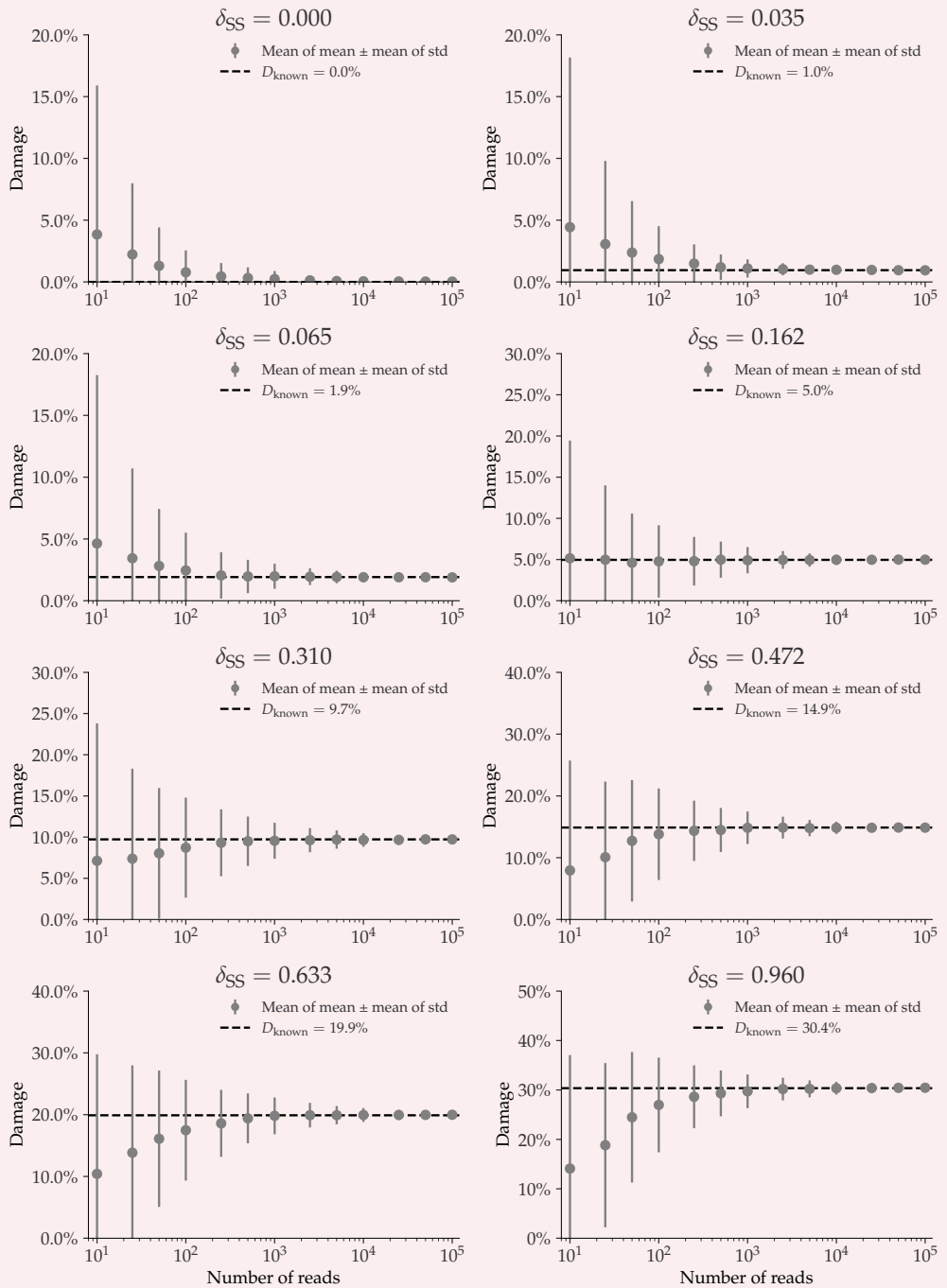
Appendix 4—figure S11. This plot shows the average damage as a function of the number of reads.

806

The grey points show the average of the individual means (with the average of the standard deviations as errors).

808

Fragment Length Average: 90



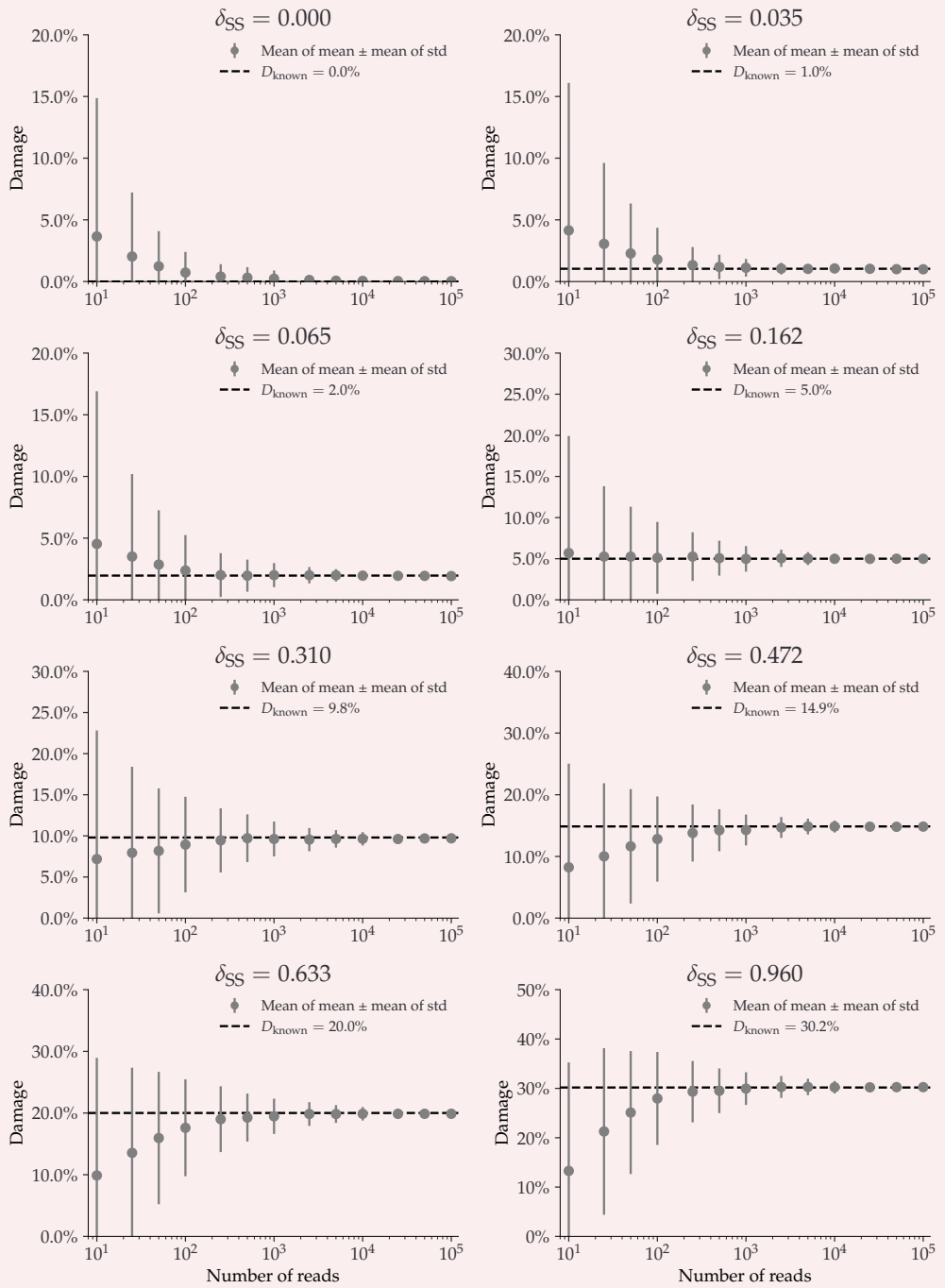
810

Appendix 4—figure S12. This plot shows the average damage as a function of the number of reads.

812

The grey points show the average of the individual means (with the average of the standard deviations as errors).

Contig length: 1 000



814

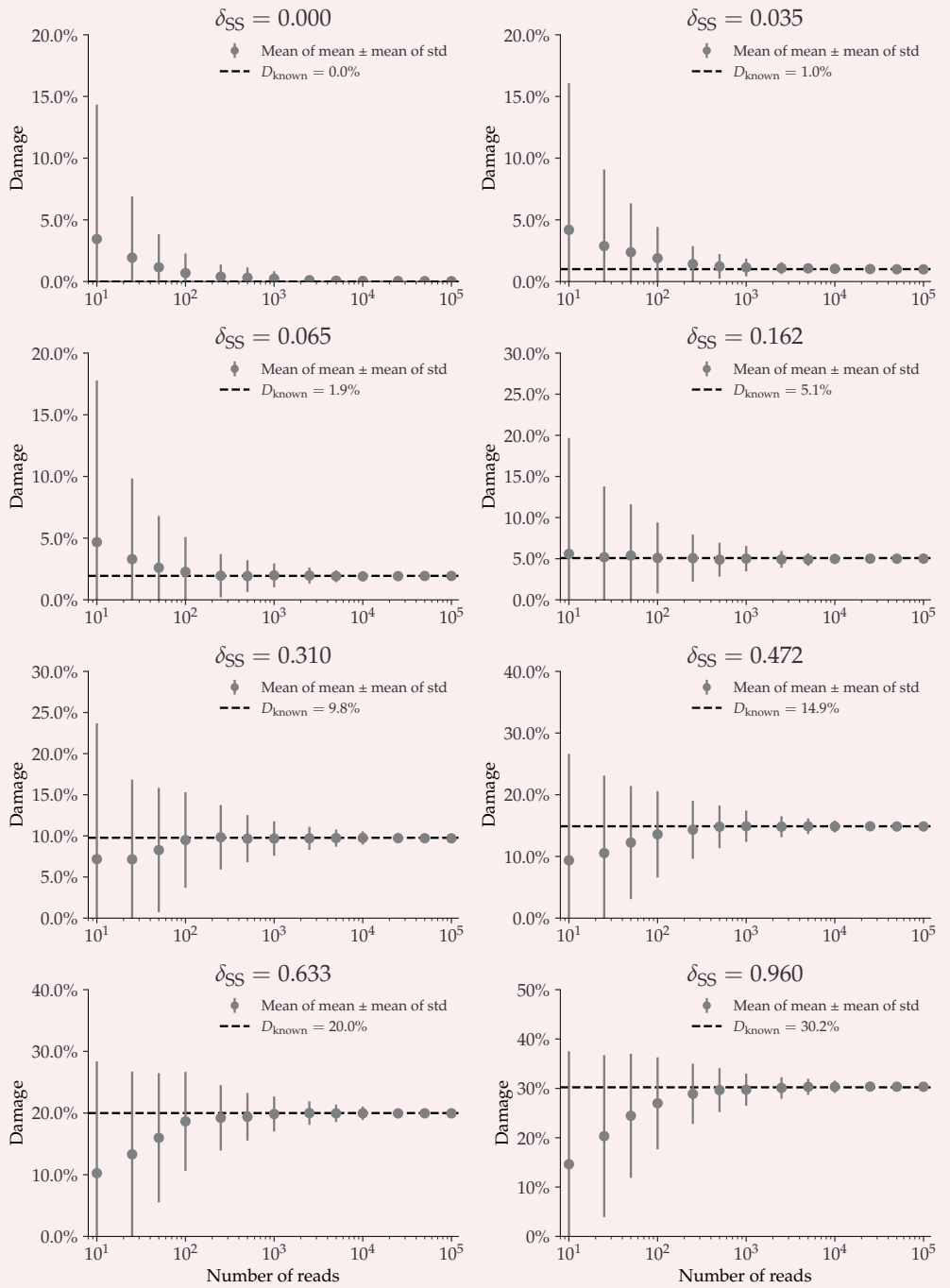
Appendix 4—figure S13. This plot shows the average damage as a function of the number of reads.

816

The grey points show the average of the individual means (with the average of the standard deviations as errors).

818

Contig length: 10 000



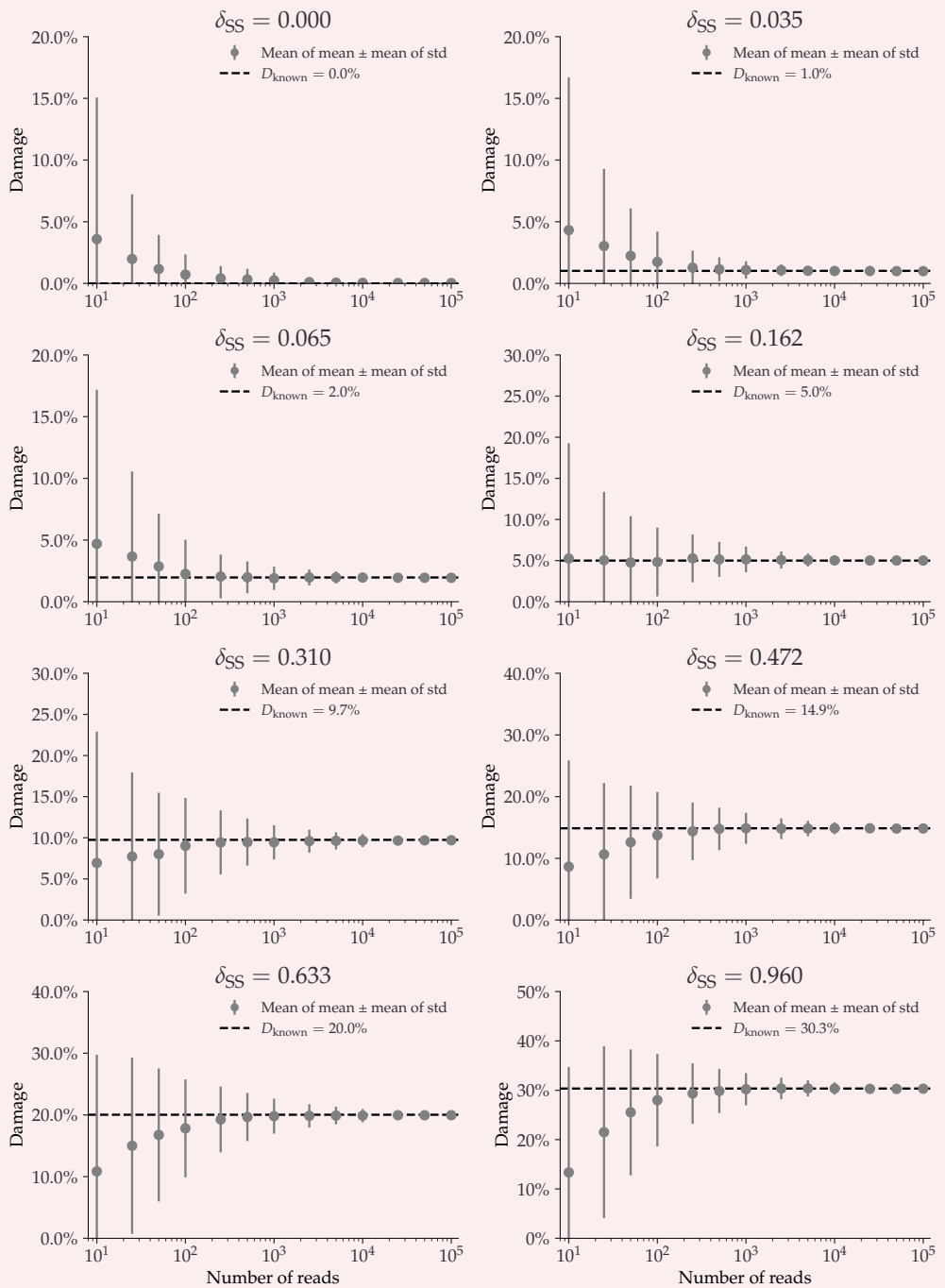
820

Appendix 4—figure S14. This plot shows the average damage as a function of the number of reads.

822

The grey points show the average of the individual means (with the average of the standard deviations as errors).

Contig length: 100 000



824

Appendix 4—figure S15. This plot shows the average damage as a function of the number of reads.

826

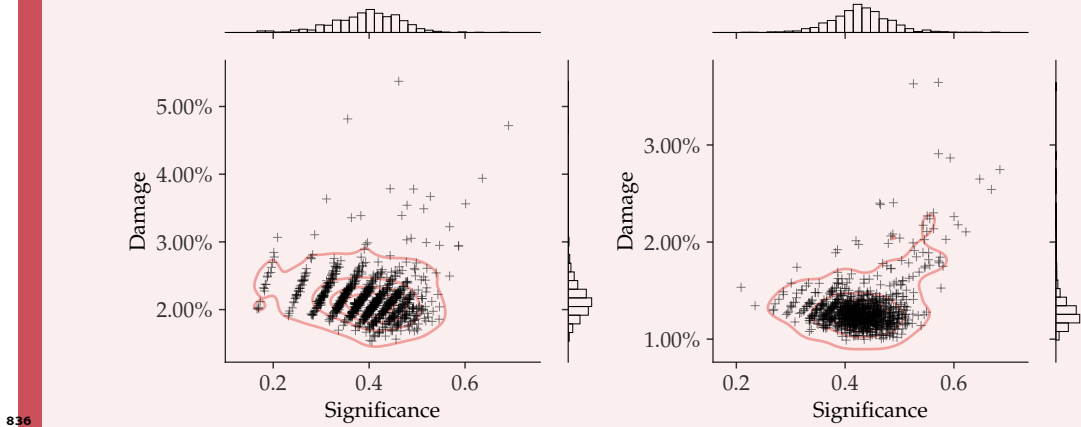
The grey points show the average of the individual means (with the average of the standard deviations as errors).

828

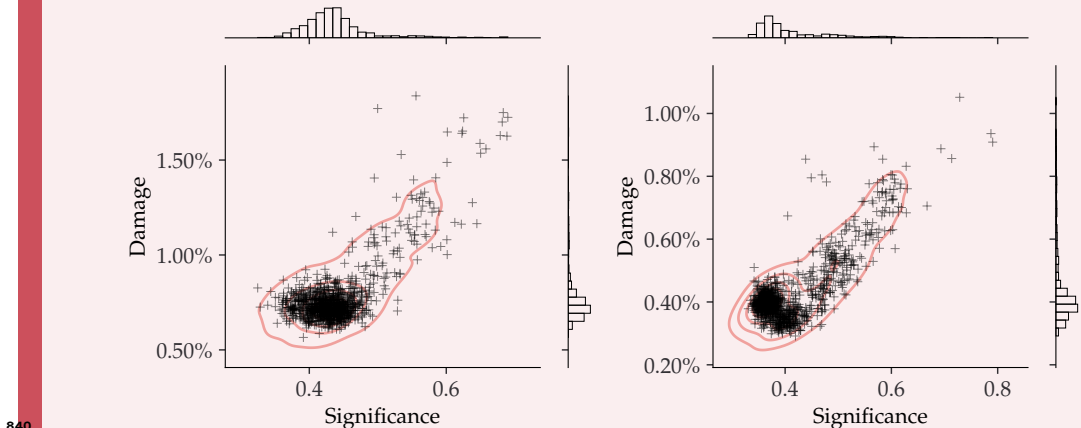
Appendix 5

NGSNGS SIMULATIONS – ZERO DAMAGE

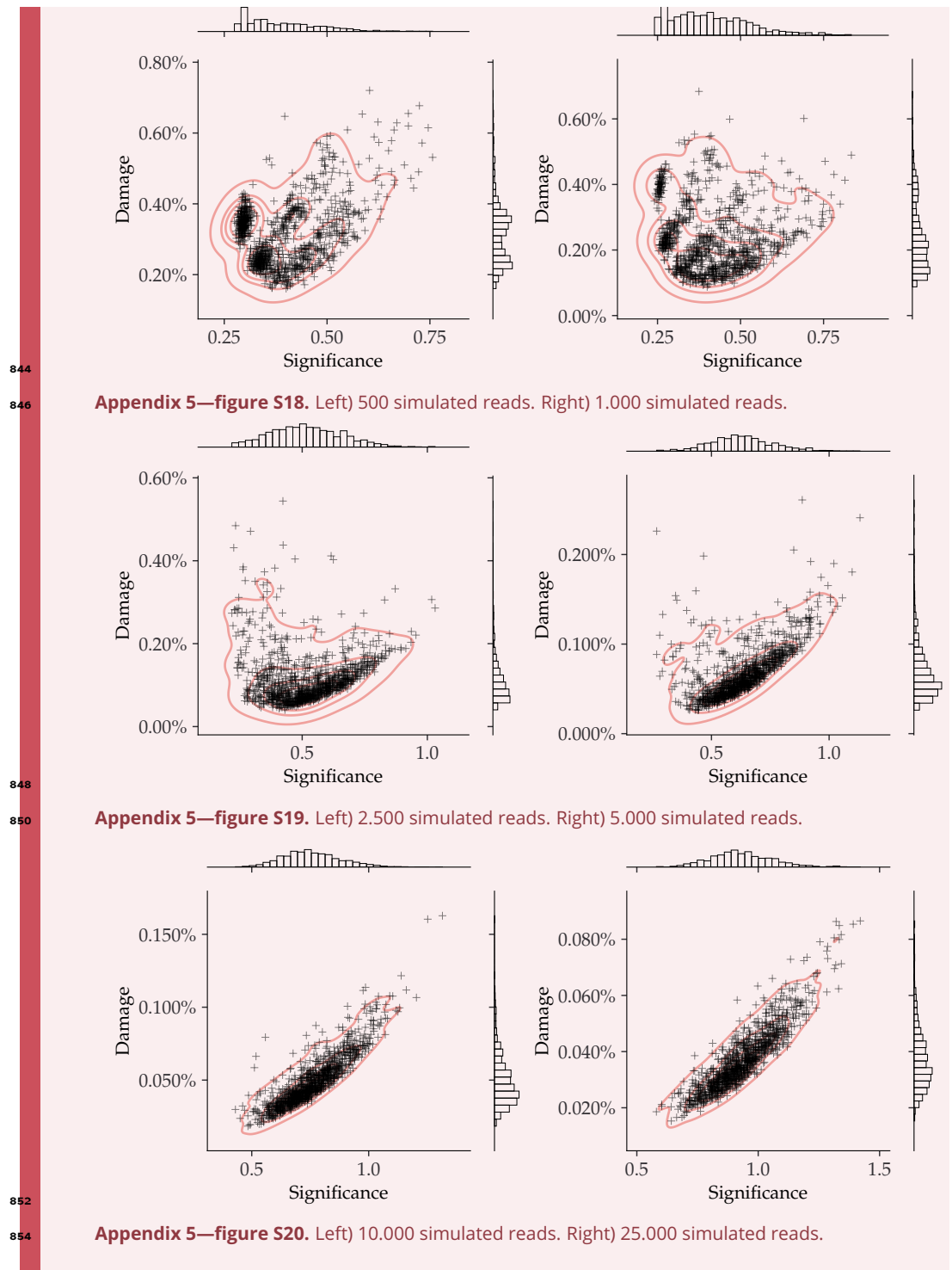
Damage estimates for non-damaged simulated data, each with 1000 replications, see [subsection 3.1](#). The inferred damage is shown on the y-axis and the significance on the x-axis. Each simulation is shown as a single cross and the red lines show the kernel density estimate (KDE) of the damage estimates. The marginal distributions are shown as histograms next to the scatter plot.

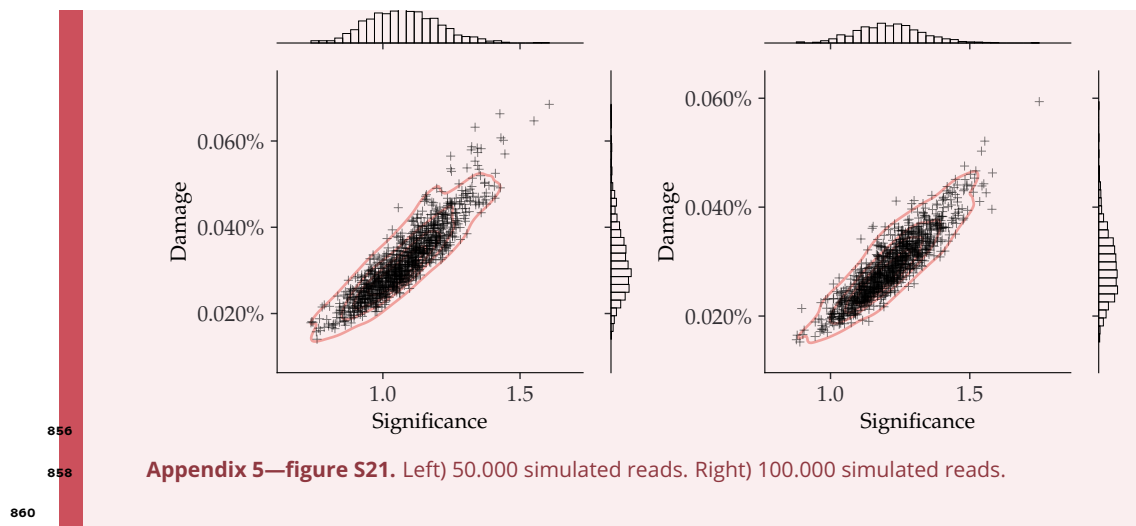


Appendix 5—figure S16. Left) 25 simulated reads. Right) 50 simulated reads.



Appendix 5—figure S17. Left) 100 simulated reads. Right) 250 simulated reads.

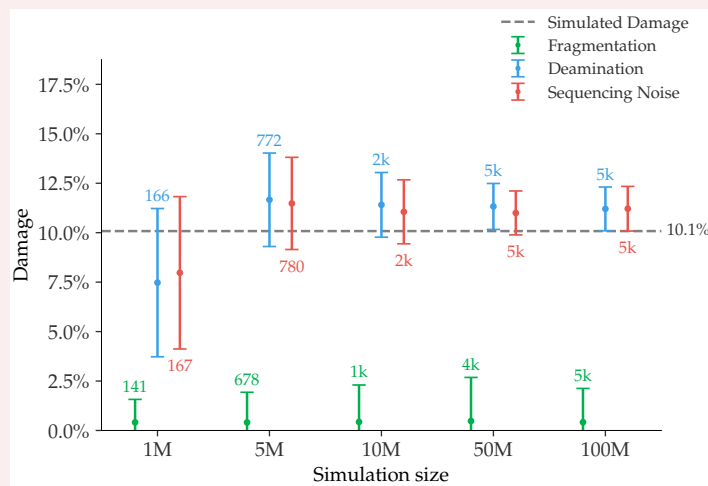




Appendix 6

FALSE NEGATIVES

Even though the simple requirement of having more than 100 reads drastically improves the performance of the damage estimates, see [subsection 4.2](#), it does not identify all of the species that were simulated to be ancient. One of these non-identified taxa is the Stenotrophomonas Maltophilia species in the Pitch-6 sample. We show the damage estimates for different simulations for this particular taxa in [Figure S22](#) to quantify the behaviour of the damage estimate at the different stages of the simulation pipeline. For the final stage in the gargammel pipeline, ie. including fragmentation, deamination, and sequencing noise (red in the figure), only 167 reads are assigned to this specific taxa after mapping, when a total of 1 million reads were simulated. The significance is $Z_{\text{fit}} = 1.9$, just below the damage threshold.

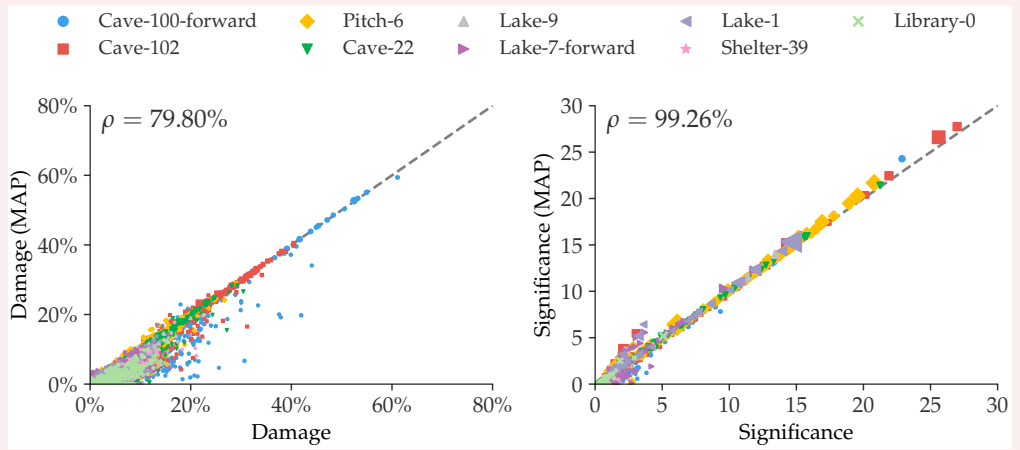


Appendix 6—figure S22. Damage estimates of the Stenotrophomonas maltophilia species from the Pitch-6 sample. Damage is shown as a function of the total simulation size, with the fragmentation files in green, the deamination files in blue and the final files including sequencing errors in red. All errors are 1σ error bars (standard deviation). The number of reads for each fit is shown as text the simulated amount of damage is shown as a dashed grey line.

882

884

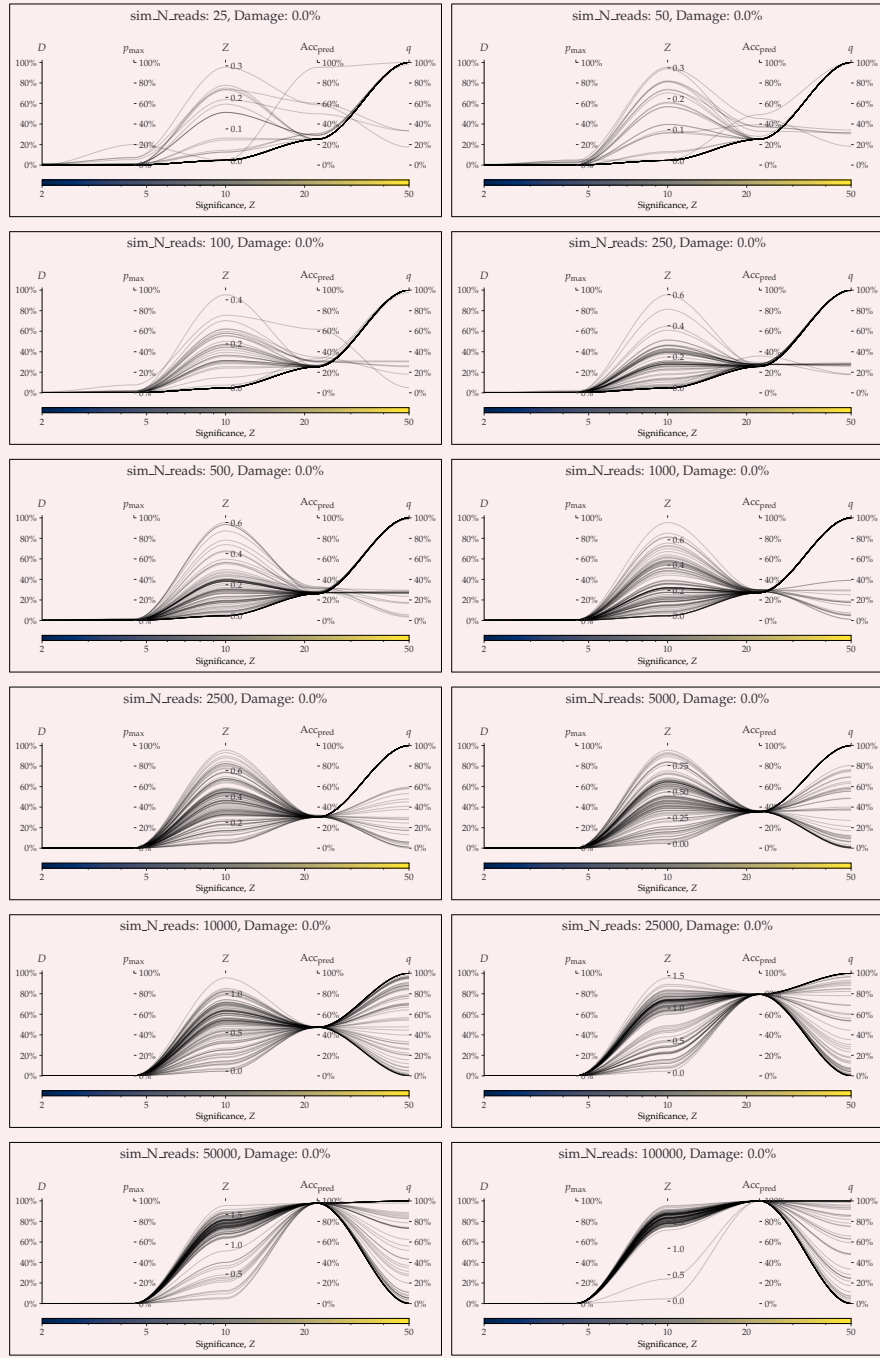
BAYES VS. MAP



Appendix 7—figure S23. Comparison between the full Bayesian model and the fast, approximate, MAP model for the estimated damage and significance. The dashed, grey line shows the 1:1 ratio.

PYDAMAGE COMPARISON

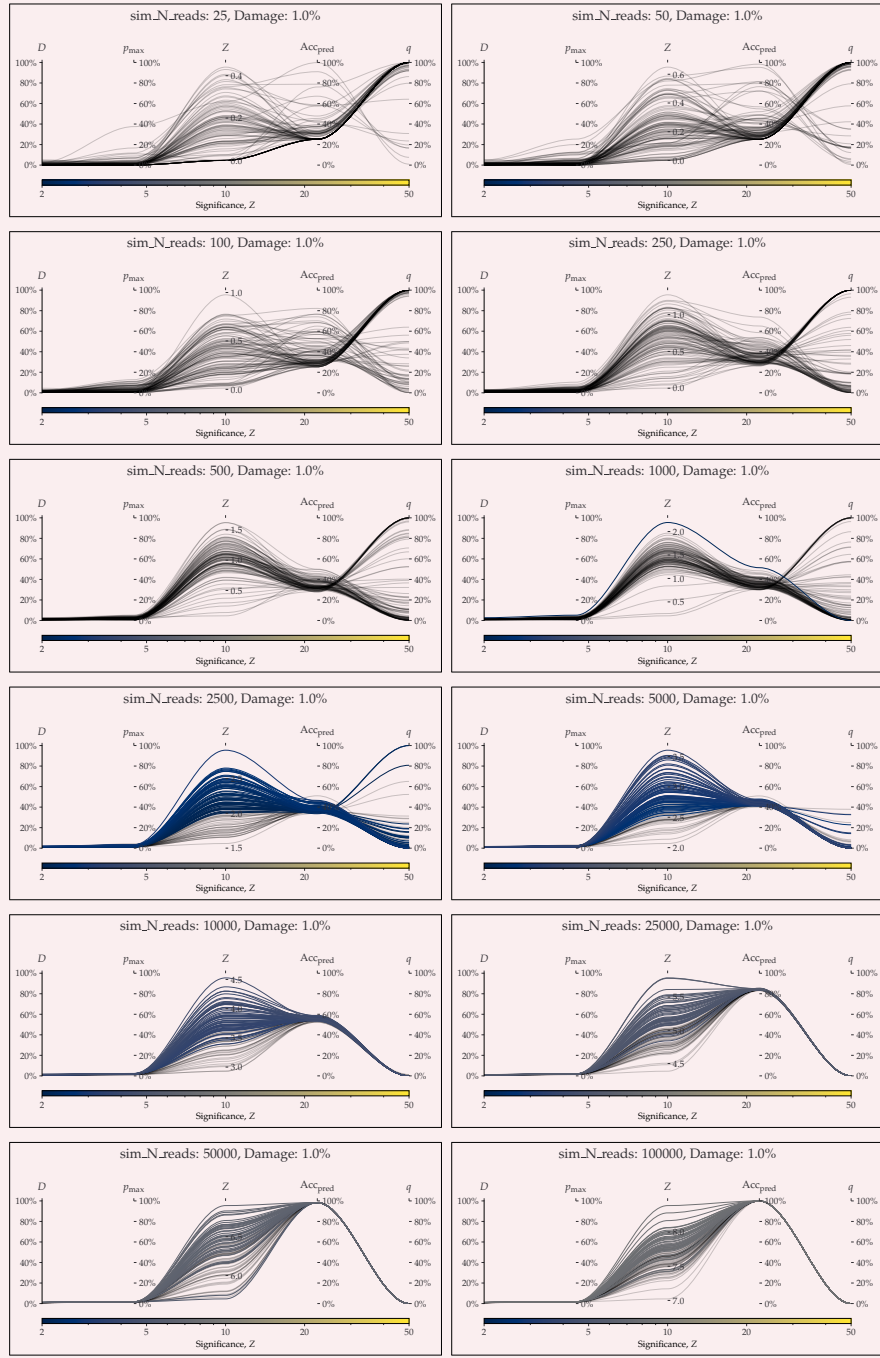
888 The following figures show the parallel coordinates plot comparing metaDMG and PyDamage
889 for the Homo Sapiens single-genome simulation with 100 reads for different amount of ar-
890 tificially added damage, see **subsection 4.5**. The two first axes show the estimated damage:
891 D_{fit} by metaDMG and p_{max} by PyDamage. The following two axes show the fit quality: signif-
892 icance (Z_{fit}) by metaDMG and the predicted accuracy (Acc_{pred}) by PyDamage. The final axis
893 shows the q -value by PyDamage. Each of the 100 replications are plotted as single lines.
894 Replications passing the relaxed metaDMG damage threshold ($D_{\text{fit}} > 1\%$ and $Z_{\text{fit}} > 2$) are
895 shown in color proportional to their significance. Replications that did not pass are shown
896 in semi-transparent black lines.



898

900

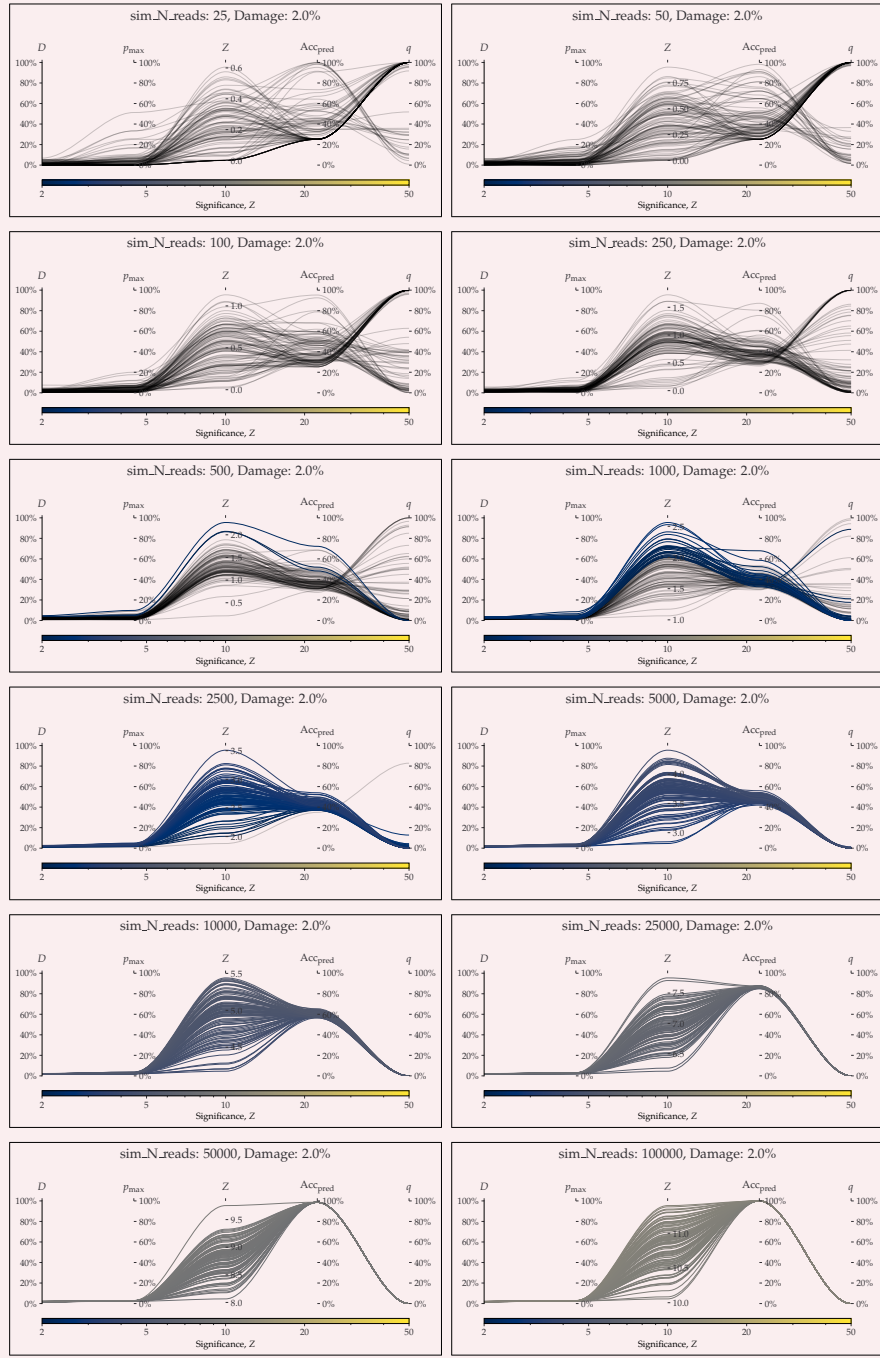
Appendix 8—figure S24. parallel coordinates plot comparing metaDMG and PyDamage for 0% artificial damage.



902

904

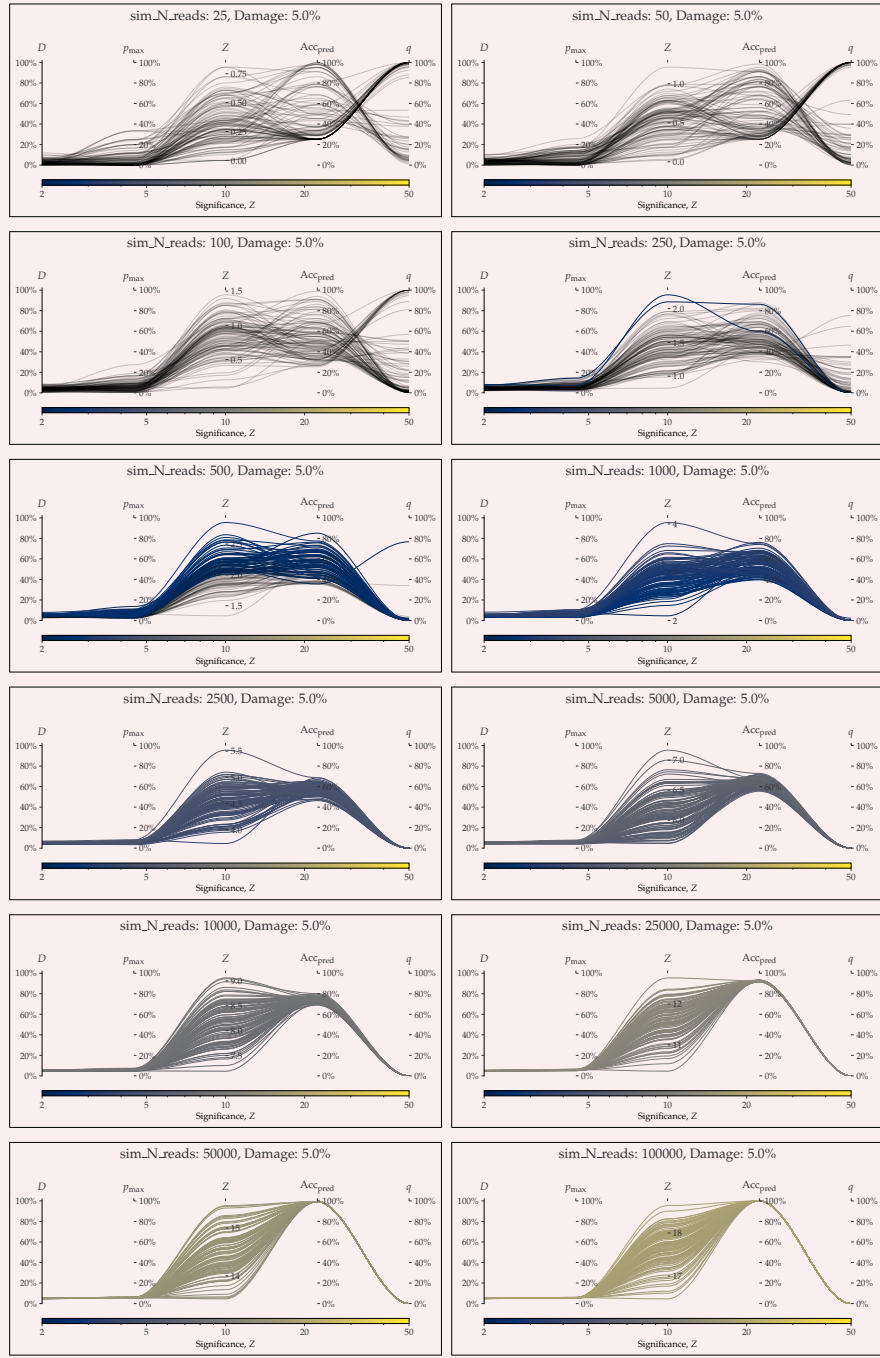
Appendix 8—figure S25. parallel coordinates plot comparing metaDMG and PyDamage for 1% artificial damage.



906

908

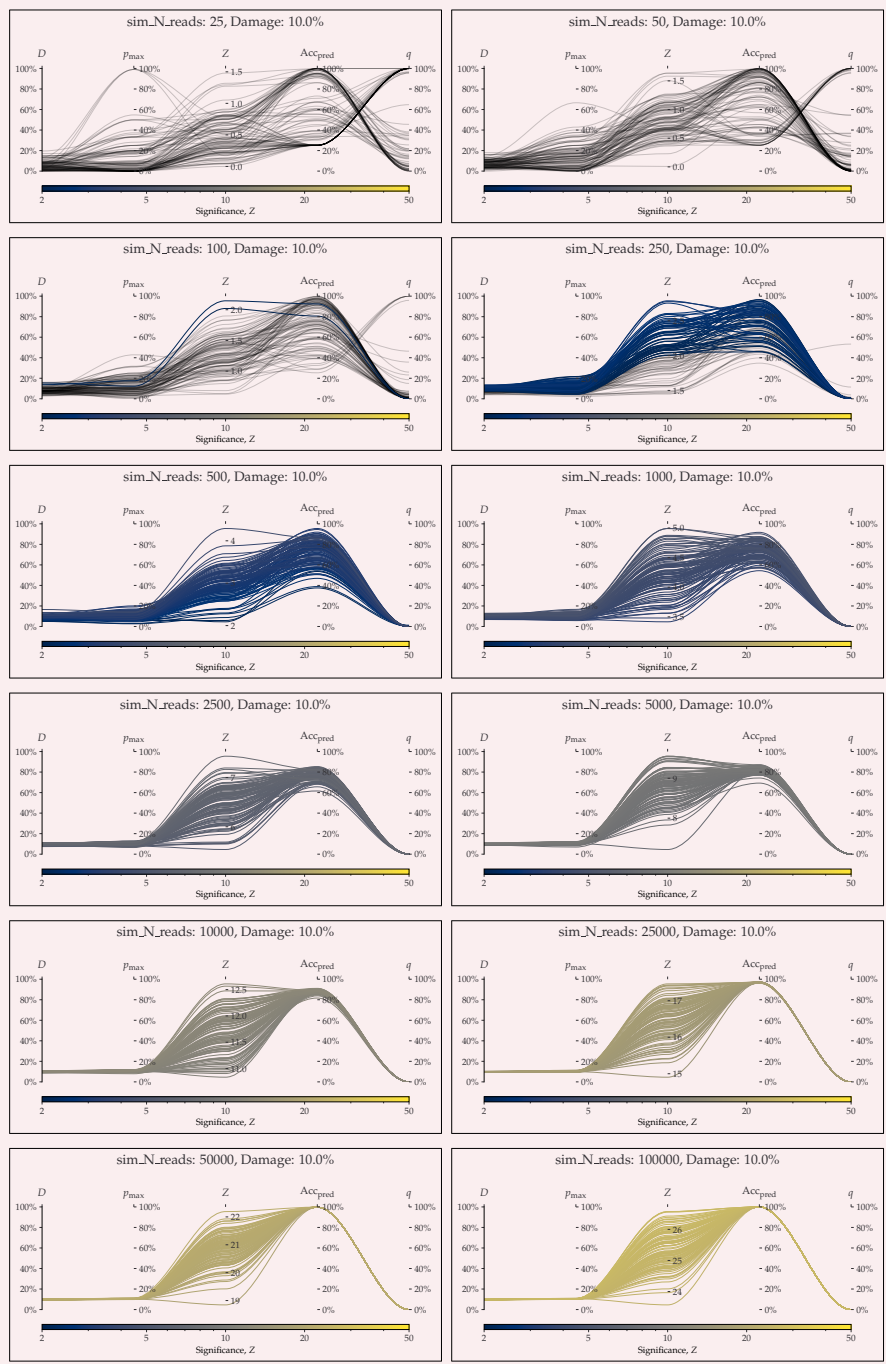
Appendix 8—figure S26. parallel coordinates plot comparing metaDMG and PyDamage for 2% artificial damage.



910

912

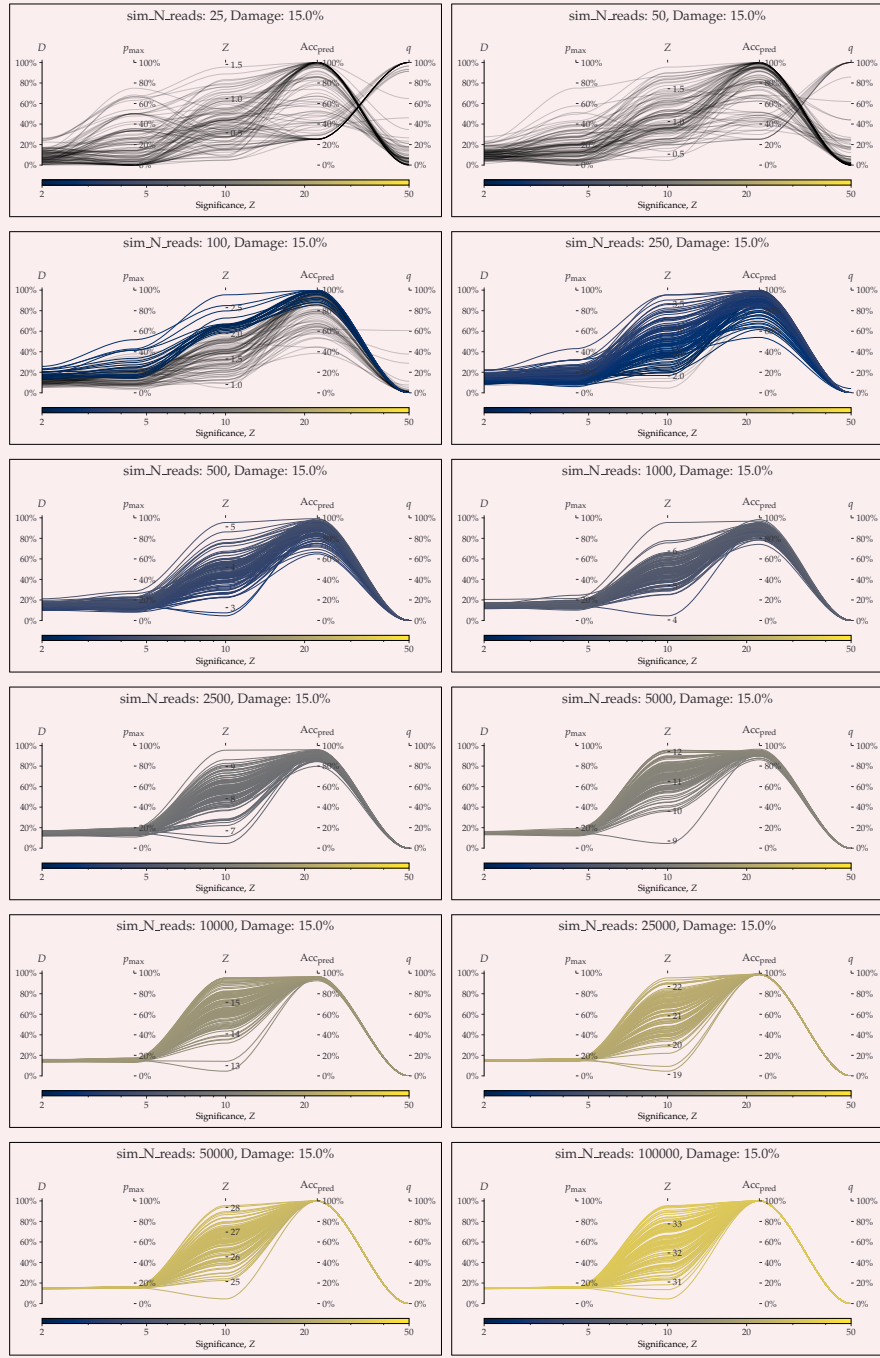
Appendix 8—figure S27. parallel coordinates plot comparing metaDMG and PyDamage for 5% artificial damage.



914

916

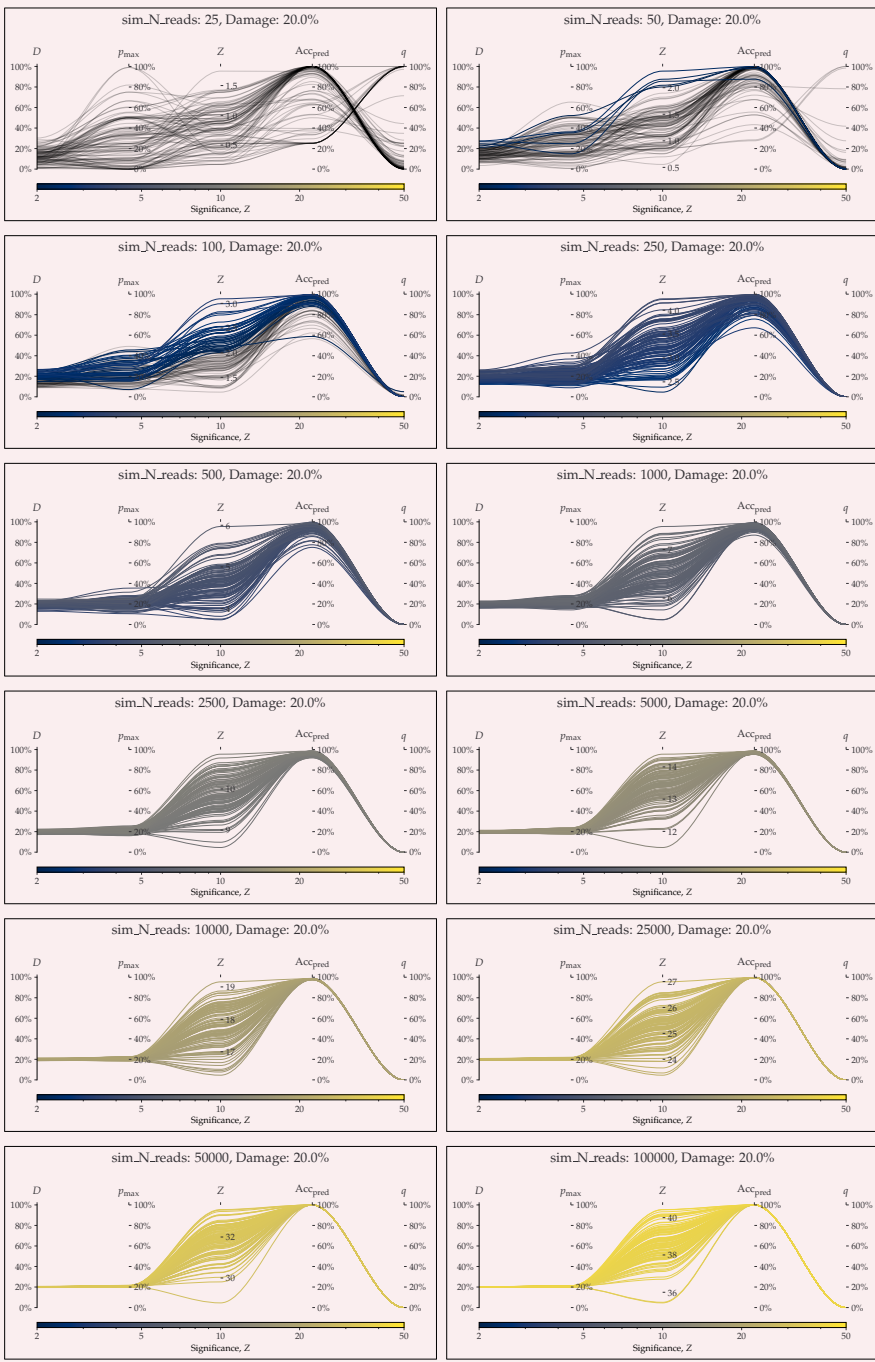
Appendix 8—figure S28. parallel coordinates plot comparing metaDMG and PyDamage for 10% artificial damage.



918

920

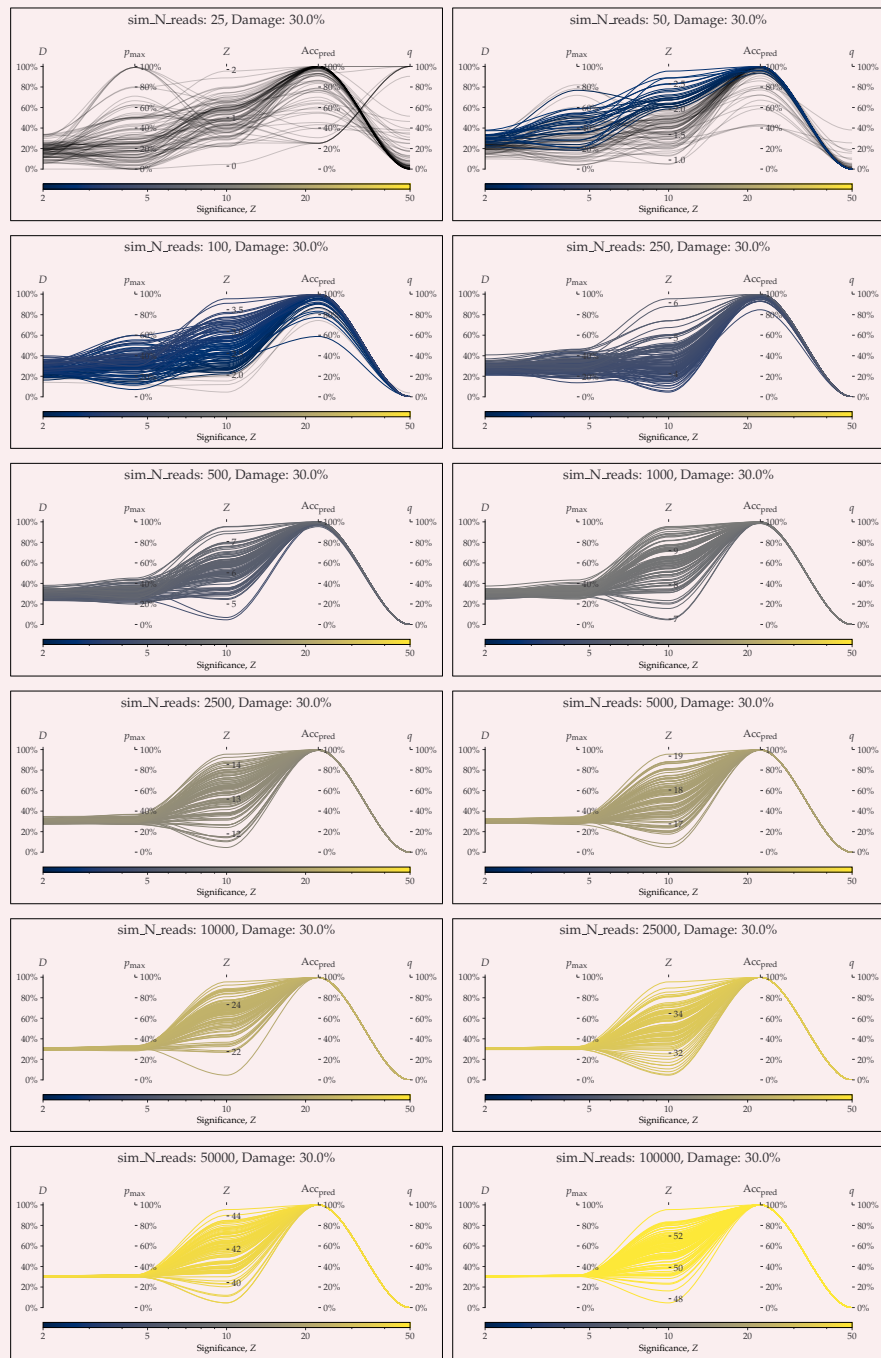
Appendix 8—figure S29. parallel coordinates plot comparing metaDMG and PyDamage for 15% artificial damage.



922

924

Appendix 8—figure S30. parallel coordinates plot comparing metaDMG and PyDamage for 20% artificial damage.



Appendix 8—figure S31. parallel coordinates plot comparing metaDMG and PyDamage for 30% artificial damage.